Marine Geology 391 (2017) 76–97

Contents lists available at ScienceDirect

Marine Geology

journal homepage: www.elsevier.com/locate/margo

Submarine canyon morphologies and evolution in modern carbonate settings: The northern slope of Little Bahama Bank, Bahamas

Elsa Tournadour[a,*,1], Thierry Mulder[a], Jean Borgomano[b], Hervé Gillet[a], Ludivine Chabaud[a], Emmanuelle Ducassou[a], Vincent Hanquiez[a], Samuel Etienne[c]

[a] Université de Bordeaux, UMR 5805 EPOC, Site de Talence Bâtiment B18N, Allée Geoffroy Saint-Hilaire, CS 50023, 33615 Pessac, France
[b] Université d'Aix-Marseille, CEREGE/UMR6635, case 67, 3, Place Victor Hugo, 13331 Marseille, France
[c] ADECAL Technopole, C/O Geological Survey of New Caledonia, DIMENC, 1 ter rue Unger, Vallée du Tir, B.P. 465, 98845 Nouméa, New Caledonia

ABSTRACT

The recent high-quality multibeam echosounder swath bathymetry data and very high-resolution seismic profiles collected along the northern slope of Little Bahama Bank (LBB, Bahamas) constitute a unique dataset that can be used to investigate submarine canyon morphologies in modern carbonate settings. This region represents one of the few examples of submarine canyons that have developed in a purely carbonate system around the world. Our study reveals that there are 18 submarine canyons within the survey area that incise the slope between water depths of 450 m and 1000 m. Morpho-sedimentary analyses allow us to characterise their geometry and spatial distribution and to interpret their formation and control parameters. Among these canyons we distinguish four types: the amphitheatre-shaped canyons (1), canyons with up-dip linear incisions (2), canyons with internal recent depositional geometries, including levees and aggrading terraces on the side of their talweg (3) and canyons that are partially to completely filled (4). Based on these new morphological and geometrical classifications, the distributions of canyon morphologies and the integration of the full dataset, we propose a model for the formation and evolution of carbonate canyons. The latter emphasises that canyon initiation is solely the result of slope failures, which subsequently evolve into proper canyons through two successive phases of retrogressive erosion processes that are controlled by a downslope submarine cementation gradient. The first phase of retrogressive erosion produces widened canyon shapes at water depths of up to 600 m, whereas the second phase forms up dip-propagating linear incisions at water depths of up to 450 m. These linear incisions, which are located 5 to 10 km away from the platform edge, favour the funnelling of sediment fluxes originating from the platform. Subsequently or contemporaneously with this retrogressive erosion, muddy gravity flows are responsible for canyon-fills and the formation of levees and aggrading terraces, which will eventually lead to the complete infill of the canyons, marking the end of an "erosion-fill" cycle. On a larger scale, the persistence of such canyons on the slope of LBB is of particular interest, as these are considered to be an exception along the present-day accretionary Bahamian slopes. Although similar canyons have been identified along the western slope of Great Bahama Bank (GBB), today these are totally buried, unlike those of LBB. We therefore suggest that the persistence of LBB canyons may be the result of relatively low sedimentation rates linked with the windward orientation of the platform. This low sedimentation rate has prevented the burial of these canyons since the Pliocene.

1. Introduction

Submarine canyons, which were originally discovered by Shepard (1936), are deep steep incisions that cut the continental shelf and slope and constitute the main conduit for the transport of sediment from the continent to the deep sea (Shepard et al., 1969; Normark and Carlson, 2003). Their initiation and entrenchment are generally closely related to erosional processes, and they may be persistent structures over long periods of time. Therefore, submarine canyons play a major role in not only sediment transfer from "source" to "sink" but also in dictating the general morphology and evolution of continental margins.

Three different processes have been proposed to explain the origin of submarine canyons: (1) precursory subaerial erosion during significant drops in relative sea level followed by submarine erosion

* Corresponding author.
E-mail address: elsa.tournadour@gouv.nc (E. Tournadour).
[1] Present address: ADECAL Technopole, C/O Geological Survey of New Caledonia, DIMENC, 1 ter rue Unger, Vallée du Tir, B.P. 465, 98845 Nouméa, New Caledonia.

http://dx.doi.org/10.1016/j.margeo.2017.07.014
Received 13 December 2016; Received in revised form 10 July 2017; Accepted 17 July 2017
Available online 21 July 2017
0025-3227/

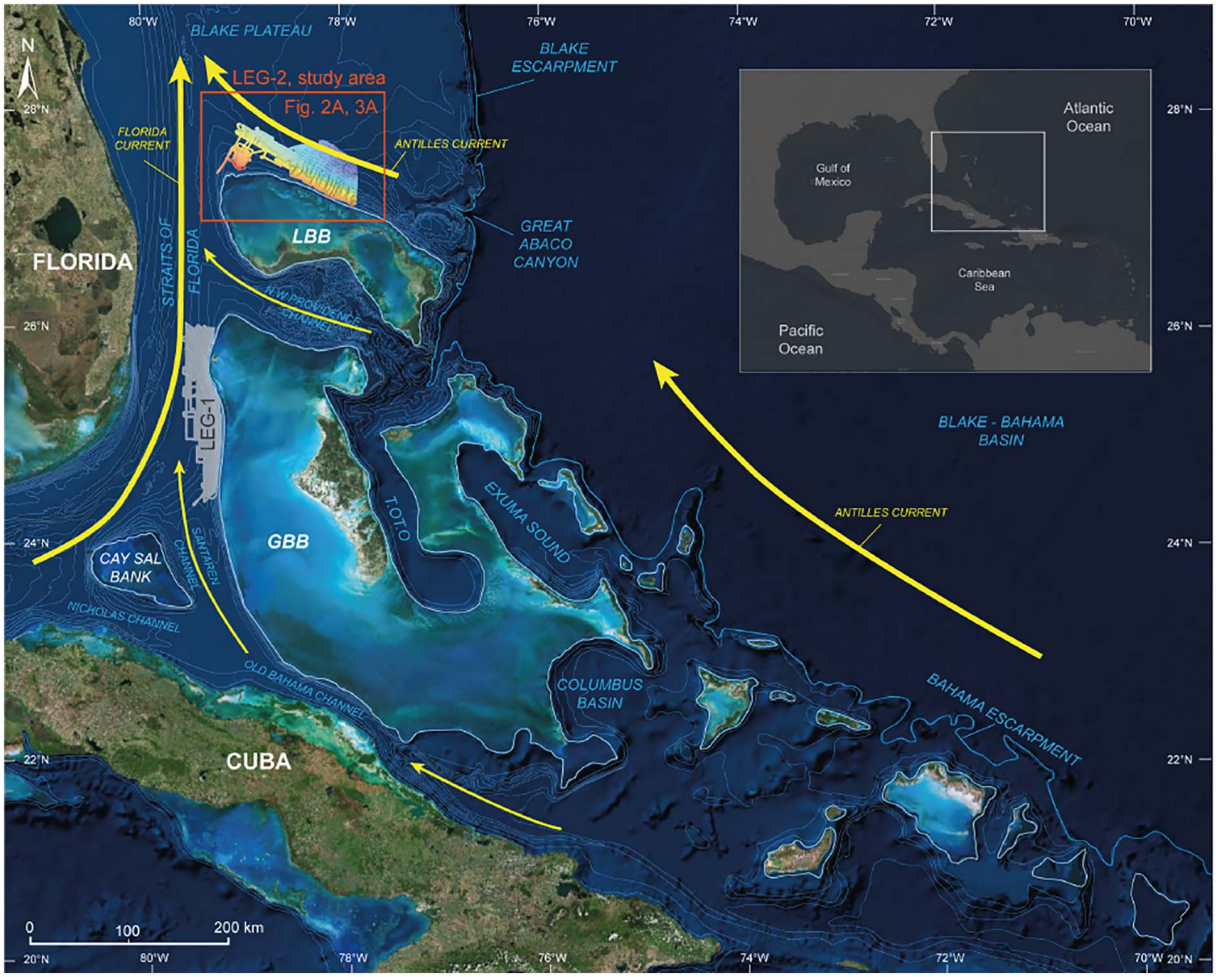

Fig. 1. Satellite image of the Bahamas archipelago and location of Leg 2 (this study, Figs. 2A, 3A) and Leg 1 of the Carambar cruise (Nov 2010, RV Le Suroit). The Antilles and Florida currents are the main oceanic currents (yellow arrows) along the Bahamas. Note that the northern slope of Little Bahama Bank marks a regional boundary between the Bahamas archipelago and the Blake Plateau. LBB: Little Bahama Bank; GBB: Great Bahama Bank; T.O.T.O: Tongue Of The Ocean. (For interpretation of the references to colour in this figure legend, the reader is referred to the web version of this article.)

(Shepard, 1981); (2) retrogressive submarine erosion linked to intra-slope destabilisation and/or downslope eroding gravity flows (Shepard, 1981; Pratson et al., 1994; Pratson and Coakley, 1996); and (3) downslope continuous submarine erosion related to recurring gravity processes, such as hyperpycnal currents generated at the mouths of large rivers (Mulder et al., 2003) or other coastal and shelf hydrodynamic processes (e.g., coastal drifts or shelf currents) (Lewis and Barnes, 1999; Canals et al., 2006; Mazières et al., 2014).

In isolated carbonate platform settings, the absence of a terrigenous fluvial system generally rules out the hypothesis of fluvial erosion during major emersion periods as well as the involvement of hyperpycnal currents associated with major floods in the origin of submarine canyons. This raises the following questions: what are the main controlling factors in the formation and evolution of submarine canyons in carbonate settings? Are they only the result of intra-slope destabilisation events and retrogressive erosion or is there any relationship between the supply and transfer of sediment from the platform and the expansion of the canyon?

These critical questions remain unanswered largely because most of the numerous studies of submarine canyons have focused on canyons in siliciclastic depositional environments (see Harris and Whiteway, 2011 and Huneke and Mulder, 2010), whereas modern submarine canyons in carbonate settings remain relatively poorly documented. However, several studies of particular note have focused on Australian continental margins (e.g., Exon et al., 2005; Mitchell et al., 2007). For example, the canyons of the Albany submarine canyon complex (offshore Southwest Australia) appear to have been inherited from siliciclastic fluvial systems that formed prior to the Middle Eocene rather than from the present-day carbonate sedimentation that fills these canyons (Exon et al., 2005). Other examples have been described in the mixed carbonate-siliciclastic systems of the northeastern Australian margin (Webster et al., 2012; Puga-Bernabéu et al., 2011, 2013, 2014). In these cases, canyon formation does not imply an initiation that is controlled by fluvial input but is instead primarily linked with intra-slope destabilisations followed by retrogressive erosion (Puga-Bernabéu et al., 2011). Additionally, along the slopes of the isolated Bahamian platforms, small fossil buried canyons and modern gully systems have also been described on the western slope of Great Bahama Bank (GBB) (Anselmetti et al., 2000; Mulder et al., 2012a; Betzler et al., 2014; Principaud et al., 2016) and the southern slope of Little Bahama Bank (LBB) (Burns and Neumann, 1987). Nevertheless, these architectural elements have been characterised using only 2D seismic lines, whereas the canyons of the northern slope of LBB have been characterised using both 2D seismic lines and a high-resolution multibeam echosounder, which can yield more detailed descriptions of canyon geometries.

In this way, the analysis of the submarine canyons on the northern slope of LBB constitute a relevant case study that can be used to understand the formation of canyons in purely carbonate settings. These features, which were originally identified as simple gullies or linear canyons by previous workers (Van Buren and Mullins, 1983; Mullins

et al., 1984; Harwood and Towers, 1988) are actually characterised by complex geometries with widened parts or amphitheatre shapes that spread upward into linear incisions. Mulder et al. (2012b) described these architectural elements and showed that canyons open on short channels and depositional fan-shaped lobes. These small turbidite systems show some similarities to siliciclastic systems. The present contribution focuses mainly on these submarine canyons; its main objective is to present a detailed morphological and sedimentary characterisation of these canyons using surface data combined with very high-resolution seismic profiles to better understand their formation and evolution, as well as their relationships to sedimentary transfer originating from the LBB platform. This detailed analysis eventually allows us to propose a new canyon classification based on their morphology, infill style, and architecture, as well as to discuss their stage of formation and their spatial distribution along the northern slope of LBB in relation to their main control parameters.

2. General settings of the northern slope of LBB

LBB is bordered to the south by the NW Providence Channel, to the west by the Straits of Florida, to the north by the Blake Plateau and to the east by the Blake-Bahama Escarpment, which marks the boundary between the Bahamas archipelago and the Blake-Bahama Basin (Fig. 1). The LBB platform is the second-largest isolated platform in the Bahamas (Fig. 1); it is 50 to 100 km wide and over 250 km long and exhibits an ESE-WNW orientation. Most of LBB is submerged; the Grand Bahama and Abaco islands represent only 15% of the total surface of the bank. The remaining 85% of the bank surface corresponds to a lagoon with a water depth ranging from 1 to 10 m. The northern slope of LBB is essentially defined as an *open ocean windward margin*; it also includes an *extended leeward margin* on its northwest extremity that has prograded northward (Mullins and Neumann, 1979). This northward progradation is the result of the growth of the LBB drift (Tournadour et al., 2015; Chabaud et al., 2016) under the combined action of the Florida and Antilles currents (Fig. 1) and represents a good example of the critical role that oceanic circulation plays in the shaping of Bahamian slopes and its associated deep-water sedimentation (Tournadour et al., 2015). The deepest part of the study area is bathed by the Labrador Sea Water, which represents the upper part of the Western Boundary Undercurrent (WBUC) (Evans et al., 2007).

2.1. Tectonic events and slope evolution

The northern slope of LBB is situated at a regional structural boundary between the Bahamas and the Blake Plateau. Its structure is closely related to the Cuban orogenesis and more particularly to the opening of the Great Abaco Canyon (Fig. 1), whose origin has been linked to the vertical motion that occurred along the Great Abaco Fracture Zone from the Upper Cretaceous to the Eocene (Van Buren and Mullins, 1983; Mullins et al., 1982). During the Paleogene, the Great Abaco Canyon was partially filled by pelagic sediments derived from a deep oceanic environment (Austin et al., 1988), thus leading to a more restricted canyon. Following this, a regional event called the “Abaco Event” led to the formation of wide destabilisations across all Bahamian slopes, together with the export of large volumes of sediment towards the Blake-Bahamas Basin from the Oligocene to the Middle Miocene (Benson et al., 1975; Bliefnick et al., 1983; Austin et al., 1988). Following this regional event, the northern slope of LBB began prograding northward; this progradation has continued until the present day (SEQ-D, Fig. 2B). ODP well 630 shows that the upper slope is mainly composed of periplatform ooze and minor chalk. During the Late Miocene, the deposition of periplatform ooze alternated with that of packstone-grainstone turbidites that formed slope apron deposits. Since the Pliocene, turbidites have constituted only 10% of the slope deposits (Austin et al., 1986) (SEQ-D, Fig. 2B). ODP well 627 is located on the lower slope and records Pliocene and Quaternary deposits that are mainly composed of periplatform oozes, with thin floatstones and minor graded packstones that have been interpreted as turbidites. The latter units are dominated by aggregates of planktonic foraminifers, contain only minor shallow-water debris and have been interpreted to be slope-derived deposits (Austin et al., 1986). The upper slope is characterised by numerous instability features, such as submarine slides, gullies and canyons (Van Buren and Mullins, 1983; Harwood and Towers, 1988; Mulder et al., 2012b; Tournadour et al., 2015) (Fig. 2). The composite seismic profile 44–57 shows that numerous incisions affected the northern slope of LBB during the Neogene (Fig. 2C). The 18 submarine canyons clearly imaged on the seafloor (Fig. 2A and Fig. 3A) incised Pliocene deposits (Fig. 2C) and consequently formed after the Late Miocene.

2.2. Platform environments

The Bahamas archipelago consists of a mosaic of isolated tropical platforms that produce both skeletal and nonskeletal carbonate sediments (Enos, 1974 and Kaczmarek et al., 2010; Purkis and Harris, 2016). The carbonate ooze platform is mainly composed of aragonite needles and magnesian calcite-rich (high Ca-Mg) deposits produced by the calcareous green algae of the lagoon (Neumann and Land, 1975). When the production of this carbonate ooze exceeds the available space on the platform, a large volume of ooze is exported to the offshore domain. During this process, platform-derived ooze is mixed with ooze produced in the water column to form what is called *periplatform ooze* (Schlager and James, 1978).

Although the sedimentary facies of the LBB inner platform is dominated by low-energy wackestones and packstones, the outer platform domain is characterised by a belt of high-energy facies that is essentially composed of oolitic grainstones associated with the development of tidal shoals (Ball, 1967; Enos, 1974 and Kaczmarek et al., 2010). The northern edge of LBB is indeed characterised by large tidal delta shoals that have developed between cays at the back of a discontinuous barrier reef (Reeder and Rankey, 2008, 2009) (Fig. 3A). These cays correspond to Pleistocene eolianite islands around which tidal currents are confined within channels (Reeder and Rankey, 2008, 2009). The associated tidal delta shoals that are present overspill lobes in both tidal directions, i.e., ebb and flood. The flow velocities measured in the tidal channels can reach up to 2 m s^{-1} and exhibit a tidal range between 0.75 m to 1 m, according to a daily tide cycle (Reeder and Rankey, 2009). This current velocity is sufficient to transport the oolitic grains, but only within the platform domain. Indeed, although the hydrodynamic regime around the shoals (i.e., the “spin cycle”) allows grain motion, this motion is spatially restricted to the region of the “oolite factory” (Reeder and Rankey, 2008).

2.3. Slope morphological features: overall characteristics

The study area begins 5 km away from the LBB platform edge at a water depth of 300 m and ends 50 km away from the platform edge at a water depth of approximately 1300 m (Fig. 3A). In the western part, the slope is approximately two times wider than it is in the eastern part and represents a prograding slope. The depositional environment in the western part is characterised by a series of complex interactions between slope destabilisations, off-bank sediment transport and longitudinal transport, as was shown by the recent study of a partially buried Mass Transport Complex (MTC) in the proximal part of this area (Tournadour et al., 2015). In contrast, the eastern part reveals a series of sedimentary bypass architectures. Indeed, approximately 40-km-long gravity systems are visible on the seafloor; these are mainly composed of 18 submarine canyons opening into the numerous distributary furrows that feed the distal confined depositional areas (Fig. 3A).

The slope of the eastern part is composed of four physiographic domains: the uppermost slope (1), the upper slope (2), the middle slope (3) and the lower slope (4) (Fig. 3B). (1) The uppermost slope extends

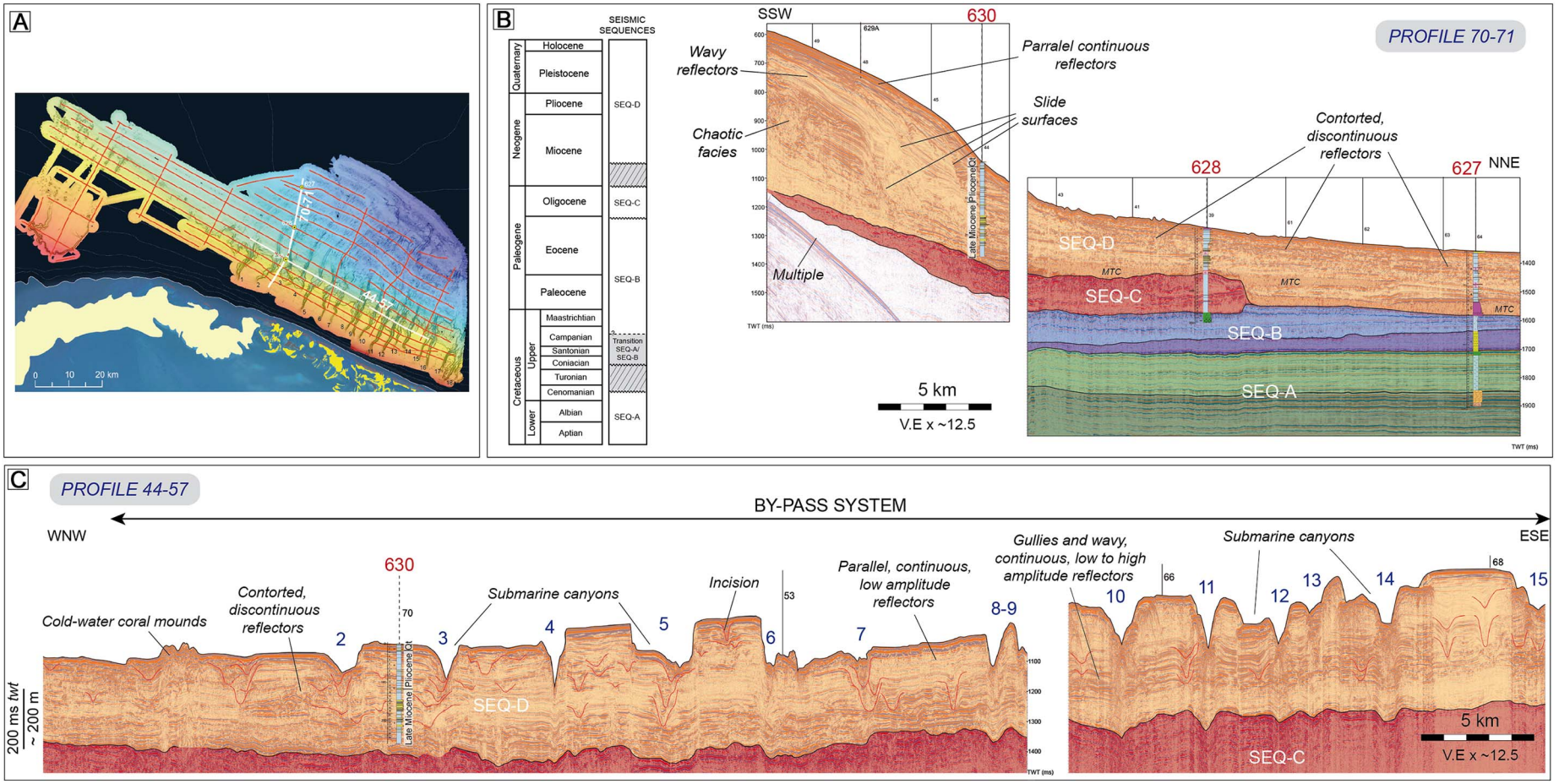

Fig. 2. Interpreted strike and dip-oriented multichannel seismic lines of the northern slope of LBB with main seismic sequences calibrated using lithostratigraphic data from ODP wells 630, 628 and 627, which penetrated Cenozoic and Cretaceous strata. (A) Localisation of the composite seismic lines 70–71 (dip line) and 44–57 (strike line) and the ODP wells on the bathymetrical map. (B) Interpreted composite seismic line 70–71. (C) Interpreted strike composite seismic line 44–57.

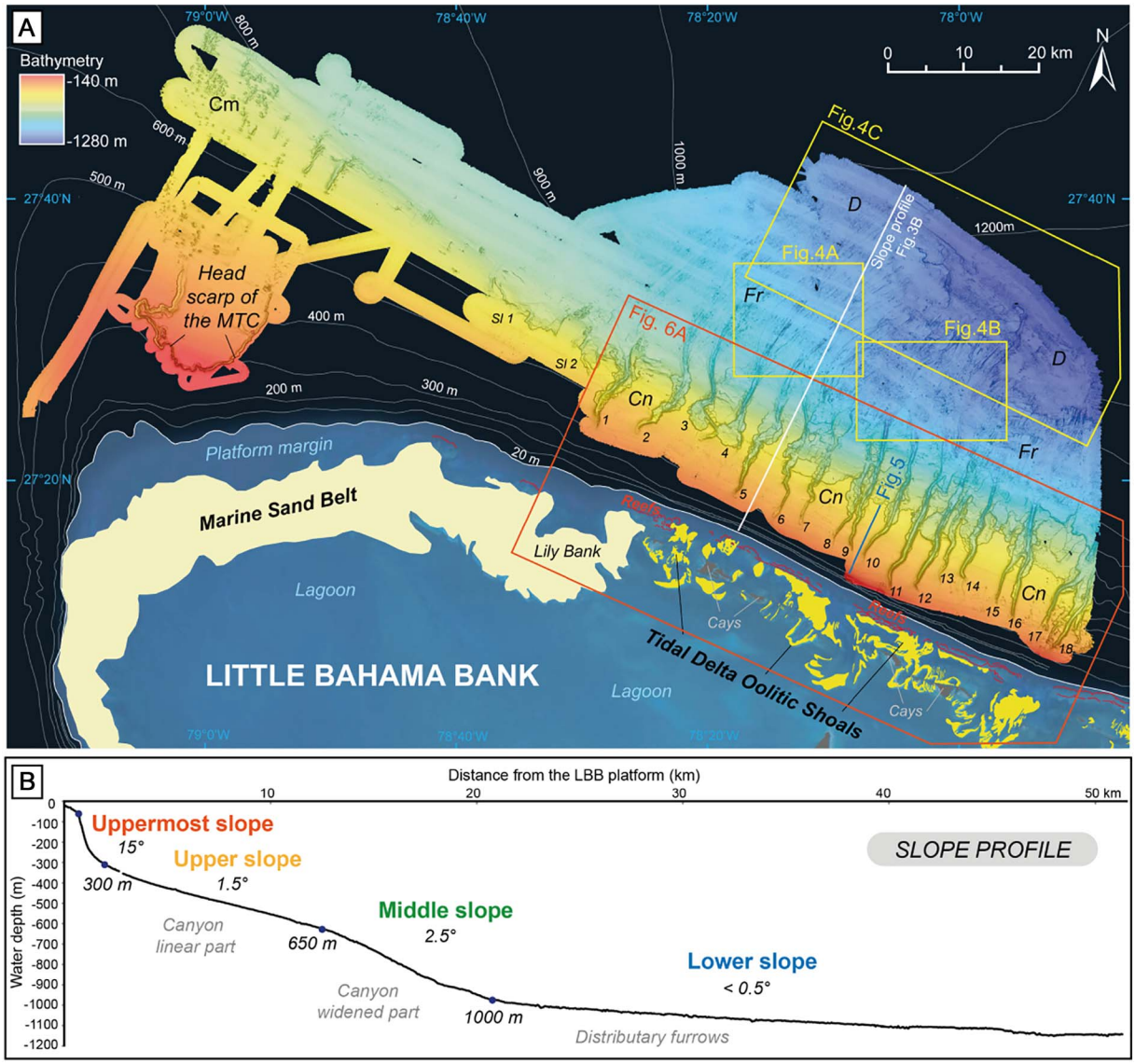

Fig. 3. (A) Bathymetrical map of the study area on the northern slope of Little Bahama Bank (LBB) and locations of the main architectural elements occurring on the slope and the main sedimentary features on the LBB platform. The study area is located 5 to 10 km from the platform edge. The northern platform of LBB is characterised by an oolitic tidal shoal at the rear of discontinuous barrier reefs. The western prograding slope displays complex interactions between off-bank sediment transport and longitudinal transport and is characterised by large destabilisations, such as a Mass Transport Complex (MTC) and submarine slides (Sl 1 and Sl 2) associated with cold-water carbonate mounds (Cm) (Tournadour et al., 2015). The eastern part is dominated by bypass architectures comprising 18 canyons (Cn) that open to distributary furrows (Fr) and feed distal depositional areas (D). (B) Typical slope profile of the eastern part of the study area. The submarine slope here is composed of four main physiographic domains: the uppermost slope, the upper slope, the middle slope and the lower slope (see text for details).

from the platform edge to a water depth of 300 m, has an average slope gradient of 15° and is characterised by several escarpments bounding terraces (Rankey and Doolittle, 2012; Mulder et al., *2017*). Downslope, at water depths ranging from 170–190 m to 300 m, the slope is covered by a carbonate ooze wedge of Holocene age that is up to 35 m thick and may have been formed by off-bank transport processes (Mulder et al., *2017*). (2) The upper slope occurs at water depths ranging from 300 m to 650 m, with an average slope gradient of 1.5° (Tournadour, 2015). The upper slope-middle slope boundary marks a change in the morphologies of submarine canyons, representing a transition from linear morphologies to wider morphologies and eventually forming amphitheatre-shaped canyons. For canyon 6, this boundary is characterised by a high escarpment (up to 100 m high) (Fig. 3A). (3) The middle slope features water depths ranging from 650 m to 1000 m and corresponds to the steepest part of the slope (with the exception of the uppermost slope), which has an average slope gradient of 2.5°. The middle slope has been affected by numerous mass transport processes. (4) Finally, below a water depth of 1000 m, the lower slope has a slope gradient of lower than 0.5° and is characterised by numerous shallow distributary furrows (i.e., 1 to 20 m deep) that developed downslope from the canyon mouths and are oriented towards depositional areas (Fig. 3A). These architectural elements are particularly distinct on acoustic imagery, where their low backscatter reveals distributary furrows and lobe-shaped depositional areas that are filled by fine-grained sediments (Fig. 4A and C) (Tournadour, 2015; Chabaud, 2016). Moreover, the acoustic imagery shows linear structures trending from N°300 to N°270 that cross-cut the distributary furrows (Fig. 4C). These sedimentary structures are interpreted to be the results of the Antilles Current, which has a SE-NW direction and was previously identified at the toe of the LBB northern slope (Chérubin, 2014; Chabaud et al., 2016), or the circulation of the deepest Labrador Sea Water (Evans et al., 2007).

Above a water depth of 1000 m, the non-eroded slope is characterised by cemented deposits exhibiting a downslope submarine

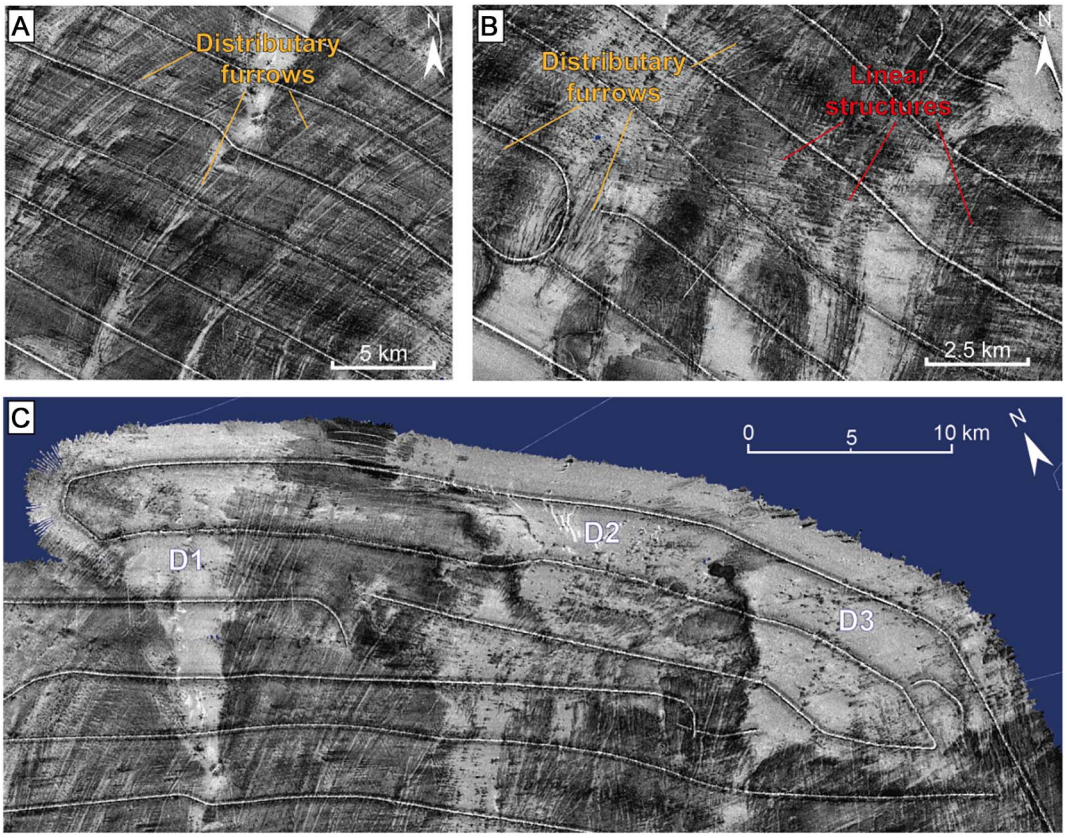

Fig. 4. Plane view of lower slope observed using backscatter imagery of water depths ranging from 1000 to 1300 m (see location in Fig. 3A) showing the following main morphological features: distributary furrows, linear structures and three depositional areas (noted D1, D2 and D3). (A) The canyon mouths open to several shallow distributary furrows that are filled by very fine-grained carbonate sand. (B) The lower slope is also characterised by erosional structures oriented from N°300 to N°270, highlighting the action of the Antilles Current action that reworks sediments towards the western part, thus contributing to the growth of the contourite LBB Drift and/or the action of the bottom Labrador Current heading towards the southeastern part of the LBB slope. (C) The distributary furrows stop on the distal lower slope in three partially confined depositional areas.

cementation gradient (Heath and Mullins, 1984; Mullins et al., 1984; Tournadour, 2015). Between water depths of 450 and 500 m, echo type analysis shows a transitional change in acoustic facies from an indistinct echo type (equivalent to echo type IIB in Mullins et al., 1984) towards a discontinuous layered echo type (equivalent to echo type IIA in Mullins et al., 1984) (Fig. 5). The first echo type cannot be calibrated using gravity core data due to the strong hardness of the seafloor. The second echo type has been calibrated using the 1.05-m-long CARKS-26 core (located on Fig. 5B). The deposits within the top 52 cm of the core are composed of silty to sandy wackestones with centimetre-size lithified nodules, whereas the basal deposits comprise intraclasts of ooze wackestones (Chabaud, 2016). This change is interpreted to represent the gradual downslope transition from a hardground facies towards a nodular ooze facies. It could be the consequence of the high diagenetic potential of the periplatform ooze and sediment winnowing by bottom currents (Heath and Mullins, 1984; Mullins et al., 1984). The periplatform ooze near the platform is mainly composed of unstable aragonite and Mg-calcite with a high diagenetic potential. Further away from the platform, the percentage of metastable minerals (aragonite and Mg-calcite) decreases; these are replaced by more stable calcite, thus reducing the intensity of submarine cementation (Heath and Mullins, 1984). Submarine slides are only present below a water depth of 500 m in poorly cemented areas. This suggests that submarine cementation controls the spatial distribution of intra-slope destabilisations (Mullins et al., 1984; Tournadour, 2015).

3. Data and methods

This study was conducted using the dataset collected during Leg 2 of the Carambar 1 cruise (November 2010 on *R/V Le Suroît*). Multibeam echosounder data were collected from an area of 5000 km^2 between water depths of 140 and 1275 m; the collected data included 3154 km of sub-bottom profiler data and Kullenberg cores.

The bathymetric map was acquired using a Kongsberg EM302 multibeam echosounder with a spatial resolution of 20 m. The acoustic imagery map was acquired with a spatial resolution of 5 m. This map reveals the backscatter of the sea bottom, whose variability mainly depends on the lithology and/or water content of the seafloor. In this study, high backscatter values are represented by dark colours (which correspond to very coarse-grained sediments and/or those with low water contents, which are usually hardened sediments), whereas low backscatter values are represented by light colours (which characterise fine-grained sands or poorly consolidated sediments). The sub-bottom profiler uses a “chirp” frequency modulated emission mode centred on 3.5 kHz. This acquisition method is characterised by an acoustic signal penetration depth ranging from 0 to 75 m and a vertical resolution ranging from 25 cm to 50 cm. This high resolution allows us to compare core lithologies with VHR seismic facies (i.e., “echo character”; Damuth and Hayes, 1977).

Three Kullenberg cores (Fig. 9) were used to calibrate acoustic facies based on their lithology and grain size. Grain sizes were measured using a Malvern Mastersizer S laser diffractometer using the Fraunhofer method. Interglacial sediments were identified in each core based on the occurrence of the planktonic foraminifer *Globorotalia menardii* (biozones Z, X and V; Ericson and Wollin, 1956; Ericson et al., 1961). Here, this biostratigraphy was used to estimate sedimentation rates. Further details of lithological facies and biostratigraphy analysis can be found in Chabaud et al. (2016) and Chabaud (2016).

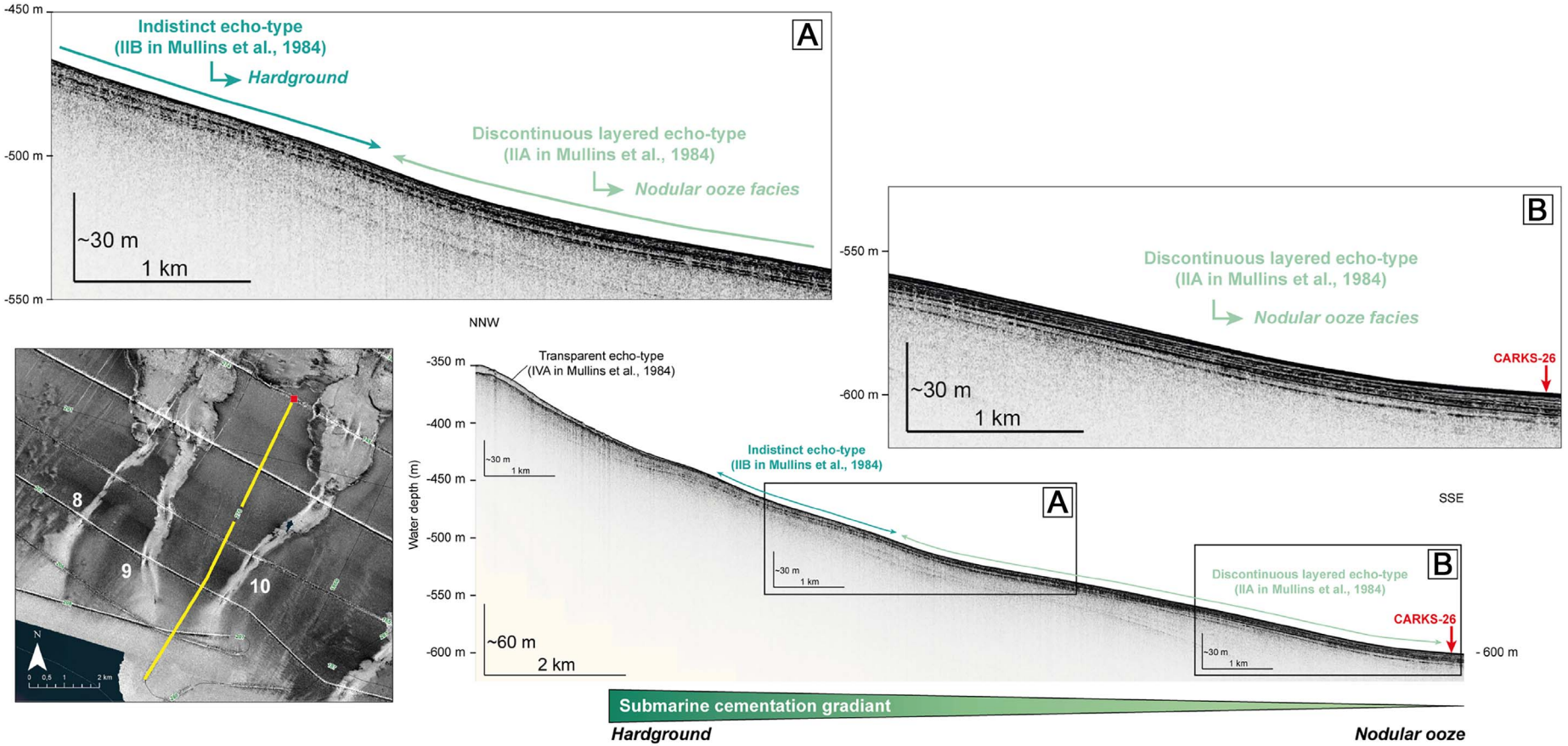

Fig. 5. Dip-oriented subbottom seismic profile along the northern upper slope of LBB from water depths of 350 to 600 m (location shown on backscatter imagery). The acoustic signal penetration increases downslope and induces a transitional acoustic facies change from an indistinct echo type towards a discontinuous layered echo type (echo-type equivalences are indicated using the classification of Mullins et al., 1984). These observations, combined with data from the CARKS 26 core and the results of the previous study of Mullins et al., 1984, suggest that this acoustic facies change corresponds to a hardground facies that gradually evolves downslope towards a nodular ooze facies.

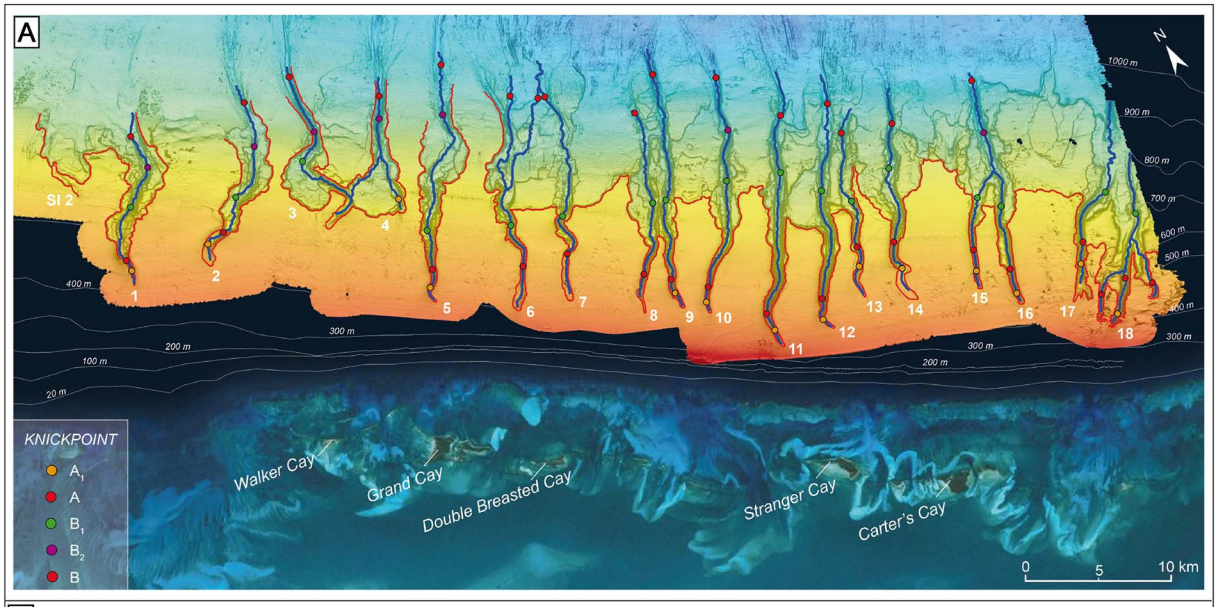

B

Canyon	1	2	3*	4*	5	6**	7	8	9	10	11	12	13	14	15	16	17	18	Average
Minimum water depth (m)	442	479	789	829	422	427	467	477	462	459	384	419	482	480	499	478	529	440	**459**
Maximum water depth (m)	834	910	955	971	998	995	981	928	1057	1024	1011	1008	911	1003	1020	1020	995		**978**
Length (km)	13.58	14.74	8.18	5.52	19.2	19.32	16.52	14.28	19.38	18.04	20.4	19.1	14.34	15.36	16.28	17.4	15.1		**17.00**
Sinuosity	1.15	1.21	1.12	1.03	1.12	1.17	1.14	1.11	1.08	1.08	1.08	1.10	1.11	1.09	1.10	1.08	1.18		**1.12**
Talweg gradient (°)	1.65	1.67	1.16	1.47	1.72	1.69	1.78	1.81	1.76	1.80	1.76	1.77	1.71	1.95	1.83	1.79	1.77		**1.76**

* These dimensions relate only to the talweg segments located outside the amphitheater-shaped areas of canyons 3 and 4, they are therefore not included in the average values.

** The talweg of canyon 6 is separated into two branches in the distal part, values of maximum water depth, length, sinuosity and slope gradient are an average of the two branches.

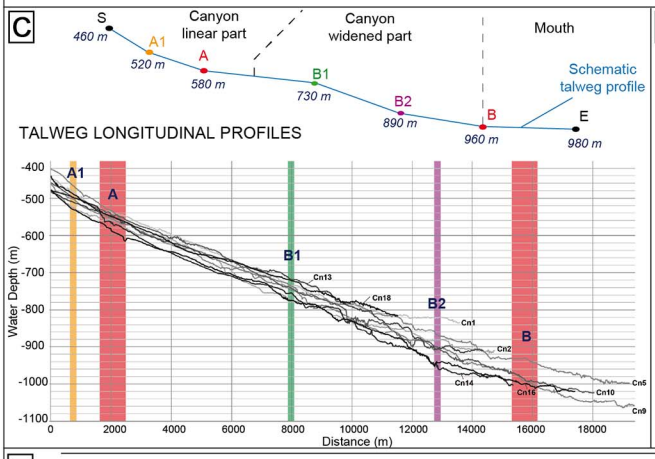

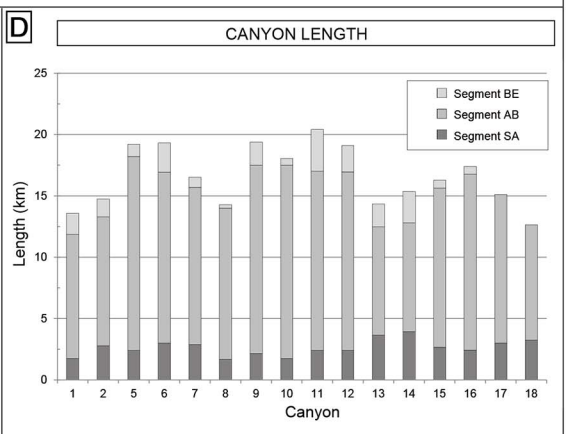

E

Canyon	1	2	5	6	7	8	9	10	11	12	13	14	15	16	17	18	Average
Linear part																	
Water depth of A (m)	533	594	564	552	556	553	560	533	506	566	612	646	615	614	692	590	**580**
SA length (km)	1.74	2.78	2.38	3	2.88	1.68	2.14	1.74	2.4	2.4	3.64	3.94	2.66	2.42	3.02	3.24	**2.63**
SA gradient (°)	3.00	2.37	3.41	2.38	1.76	2.58	2.61	2.44	2.91	3.52	2.05	2.42	2.49	3.20	3.08	2.66	**2.68**
Widened part																	
Water depth of B1 (m)	685	699	671	644	662	747	740	801	827	809	695	795	702	727	784	725	**732**
Water depth of B2 (m)	774	834	921					934					945	945			**892**

Fig. 6. Bathymetrical analysis data and main morphological parameters of LBB submarine canyons. (A) Bathymetrical map showing the 18 canyons incising the northern LBB slope (see location in Fig. 3A). Canyon boundaries are represented by red lines and their talwegs are indicated by blue lines. (B) Main physical parameters of LBB submarine canyons, including minimum and maximum water depths, sinuosity and talweg slope gradient. (C) Talweg longitudinal profiles of nine canyons and schematic talweg longitudinal profile from canyon start (S) to canyon end (E). Talweg profiles are organised following several knickpoints (noted A, A1, B, B1 and B2) that delimit specific morphological sections (see explanations in the text). (D) Histogram of canyon lengths. (E) Physical parameters of the linear and widened parts of submarine canyons. (For interpretation of the references to colour in this figure legend, the reader is referred to the web version of this article.)

4. Results

4.1. General canyon morphologies

Between water depths of 450 m and 1000 m, the eastern part of the study area is incised by 18 submarine canyons (among the 22 described by Mullins et al., 1984), which show strong morphological variability from west to east (Fig. 6A). Slope-confined canyons 1 to 5 are well-delimited, whereas it is difficult to differentiate individual canyons to the west of canyon 6, as their interfluves are not preserved. Along the upper slope, all canyons are characterised by linear morphologies above water depths of 650 m, with the exception of canyons 3 and 4, which exhibit amphitheatre shapes (Fig. 6A). The quantitative analysis of the morphological parameters of these canyons reveals that they have an average length of 17 km, a straight shape (with an average sinuosity of 1.12) and a talweg slope gradient that ranges from 1.65° to 1.95° (Fig. 6B).

The analysis of talweg longitudinal profiles allows us to identify several knickpoints that longitudinally subdivide canyons. The first major knickpoint, noted A, is located in the proximal part of the linear incisions at an average water depth of 580 m (Fig. 6C). In addition, for descriptive purposes, the start and end points of the talwegs are defined as “S” and “E”, respectively. Segment SA is a restricted section of the whole talweg profile (Fig. 6D) and ranges in length from 1.7 km to 4 km. It also records a high gradient contrast compared to the rest of the profile, as it has an average slope of 2.68° (Fig. 6E) and could therefore conform to the canyon “headwall”. The second major knickpoint, noted B, corresponds to the canyon mouth and is associated with a decrease in the inclination of the slope. Two other knickpoints that are less well pronounced, which are noted B1 and B2, are present in some canyons. They are located in approximately the middle parts of the canyons (Fig. 6C) at average water depths of 732 m and 892 m, respectively (Fig. 6E). They record clear morphological changes in the widened sections of the canyons. B1 marks the enlargement of the canyons, defining a sharp contrast with the linear canyon that extends along the upper slope (Fig. 6A). Knickpoint B2 seems to mark the narrowing of the canyon width before its mouth (Fig. 6A).

A map of canyon incision depth (Fig. 7) was computed based on the subtraction of an extrapolated non-eroded slope surface from the present-day bathymetry. This map enables us to display only the incision depth of the canyons by removing the water depth. This analysis highlighted the following morphological characteristics: shallow incision in the linear part, the presence of terraces bordering the talwegs and the occurrence of downslope erosion areas showing partially channelised linear shapes (Fig. 7).

4.2. Canyon typology

Among the 18 canyons in the study area, four main types have been distinguished based on morphological criteria, such as their amount of fill, degree of talweg confinement, general shape and terrace/levee geometries. Type 1 and 2 canyons correspond to unfilled and slope-confined canyons, as well as those with well-delimited morphologies. Type 1 canyons end in the middle slope with an amphitheatre shape, whereas type 2 canyons exhibit up-dip linear incisions. In contrast, type 3 and 4 canyons are filled to various degrees. Type 3 canyons represent an early infill stage with levees and aggrading terraces and are differentiated from type 4 canyons, which are partially or totally filled.

4.2.1. Amphitheatre-shaped canyons

Unlike other canyons, canyons 3 and 4 do not have proximal linear parts but instead end in wide “amphitheatres” (3 to 4 km in diameter) that are delimited by escarpments that can reach heights of up to 100 m and are marked by several arcuate scarps (Fig. 8A, B and C). The amphitheatre-shaped parts of these canyons, which are located at water depths between 550 and 700 m, lead to narrow V-shaped valleys that are only 700 m wide (profiles c and d, Fig. 8E). The amphitheatre-shaped parts of canyons 3 and 4 are connected by a channel that is approximately 60 m deep. The latter is connected to the upper slope through canyon 4 (Fig. 8A and B). Between canyons 3 and 4, many scarps are present in the interfluve area, where several 10- to 20-m-high mounded structures have developed; these are interpreted to be cold-

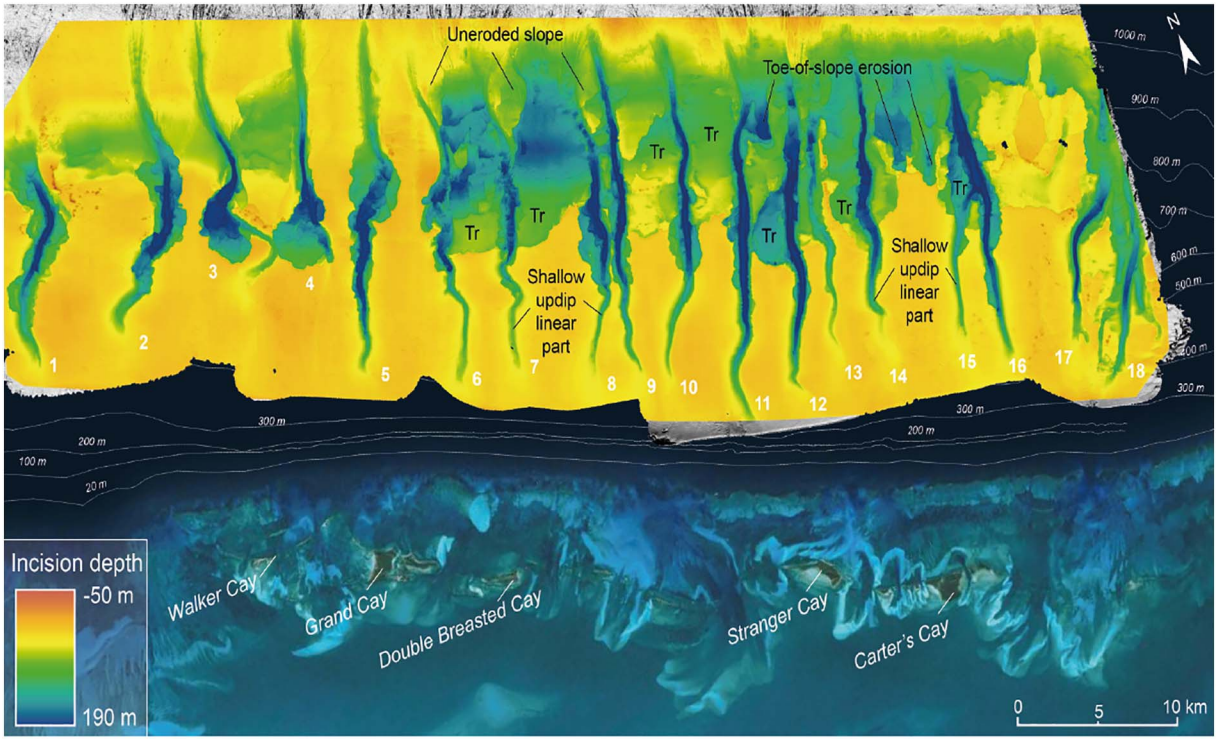

Fig. 7. Canyon incision depth map obtained by the subtraction of an extrapolated uneroded slope surface from the present-day bathymetry. This map highlights the shallow linear incisions of the upper slope, the occurrence of terraces (Tr) within canyons, and areas of the preserved (i.e., uneroded) middle slope and linear or angular toe-of-slope erosions.

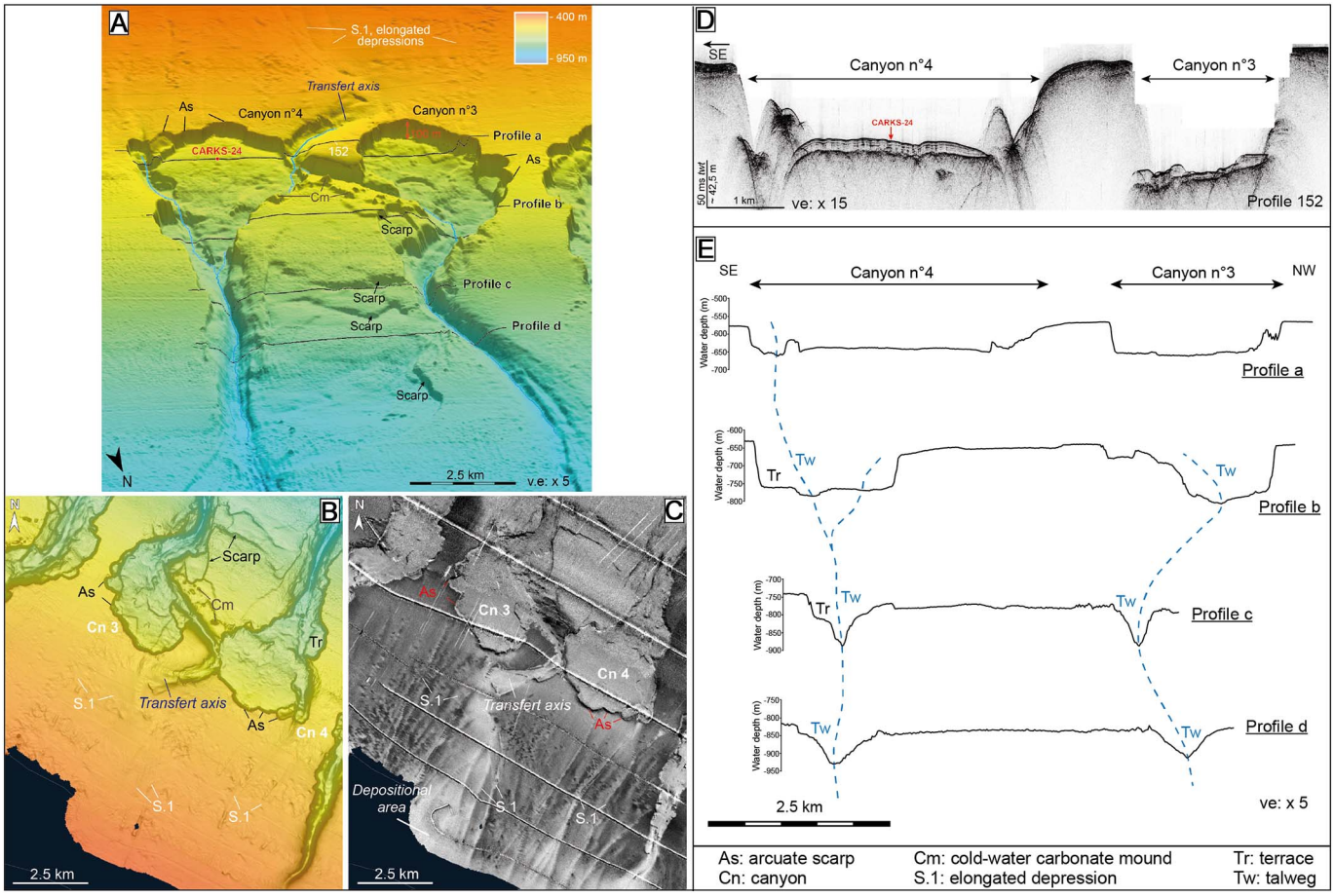

Fig. 8. Detailed characterisation of amphitheatre-shaped canyons (e.g., canyons 3 and 4). (A) 3D bathymetrical map of canyons 3 and 4 and their associated morphological features. (B) Plan view of bathymetrical map of canyons 3 and 4. (C) Plan view of backscatter imagery of canyons 3 and 4. (D) Chirp seismic profile 152 crossing canyons 3 and 4 in their proximal, amphitheatre-shaped part. Note the location of the CARKS-24 core (see Fig. 9). (E) Representative bathymetric cross-sections (noted a to d) along canyons 3 and 4, moving from their proximal amphitheatre-shaped parts to their mouths. Both canyons start at a water depth of approximately 550 m with a wide amphitheatre-shaped area, the edges of which are affected by several arcuate scarps. These two widened sections are connected to each other and the upper slope by a channel that is believed to funnel platform-derived sediments. As: arcuate scarp; Cm: cold-water carbonate mound; Tr: terrace; Cn: canyon; S.1: elongated depression; Tw: talweg.

water carbonate mounds (Fig. 8A and B).

Within the proximal parts of the amphitheatre, a *c.* 10-m-thick sedimentary infill is visible and is characterised by a layered echo type on chirp profiles (Fig. 8D). The lithology of the 7.57-m-long CARKS-24 core (Fig. 9) that was located in the amphitheatre-shaped part of canyon 4 (Fig. 8A and D) essentially comprises silty mud wackestone and, in some places, intervals of normally graded fine- to medium-grained carbonate sands. These deposits have been dated to the MIS-5 stage (< 120 ka) with sedimentation rates of > 15 cm/ka during interglacial periods and those of a few cm/ka during glacial periods (Chabaud, 2016).

In addition, up dip of canyons 3 and 4, the bathymetrical map displays 1- to 2-m-deep downslope shallow linear structures, some of which are captured in amphitheatre-shaped areas (S.1, Fig. 8A and B). These structures are typically 2–3 m deep and 50–100 m wide; they are better imaged on EM302 imagery, on which they clearly appear to be filled with low-backscatter deposits (S.1, Fig. 8C). Of particular note is the presence of a spreading depositional area evidenced by low backscatter that is associated with S.1 structures that seem to extend towards the channelised axis between canyons 3 and 4 (Fig. 8C). Based on these new observations and those of previous studies (Mullins et al., 1984; Rankey and Doolittle, 2012; Mulder et al., 2017), these structures are interpreted to represent downslope transfer axes of periplatform ooze.

4.2.2. *Canyons with up-dip linear parts*

This type of canyon is typified by canyons 1, 2 and 5, which comprise an up-dip linear part and non-eroded interfluves. Canyon 5 is a very good example of this morphological type (Fig. 10). This slope-confined, 19-km-long canyon is limited by its steep edges, which are up to 80 m high and comprise numerous coalescing arcuate scarps (Fig. 10A). The canyon begins with an up-dip linear incision that cuts the upper slope (see cross-section profiles a and b in Fig. 10B) and widens along the middle slope, where it ranges in width from 1.2 km to 3 km (profiles b and c). Finally, the canyon narrows again at a water depth of 900 m, from 3 km to 1.5 km wide (profile d). The talweg incision profile reveals that the maximum depth (150 m) is reached in the widest part of the canyon, along the middle slope (Fig. 10C). The inner part of the canyon is characterised by terraces with an elevation of approximately 50 m above the bottom of the talweg. In this case, they are especially well developed; they can reach up to 1.5 km wide and extend over 3.5 km long (profile c, Fig. 10B).

The inner part of canyon 5 can be observed using the four chirp profiles located close to the bathymetrical cross sections provided in Fig. 10B. These profiles reveal that all talweg floors are covered by soft sediments, except in the up-dip linear incisions (profile 208). Canyon terraces (profile 146) and some edges (profiles 152 and 146) comprise deposits generating a slightly layered echo type, with some hyperboles present in the steepest areas. These deposits, which are interpreted as periplatform ooze, are relatively thin but can reach thicknesses of up to 20 m (approximated using an average velocity of 1700 m s^{-1}) in the

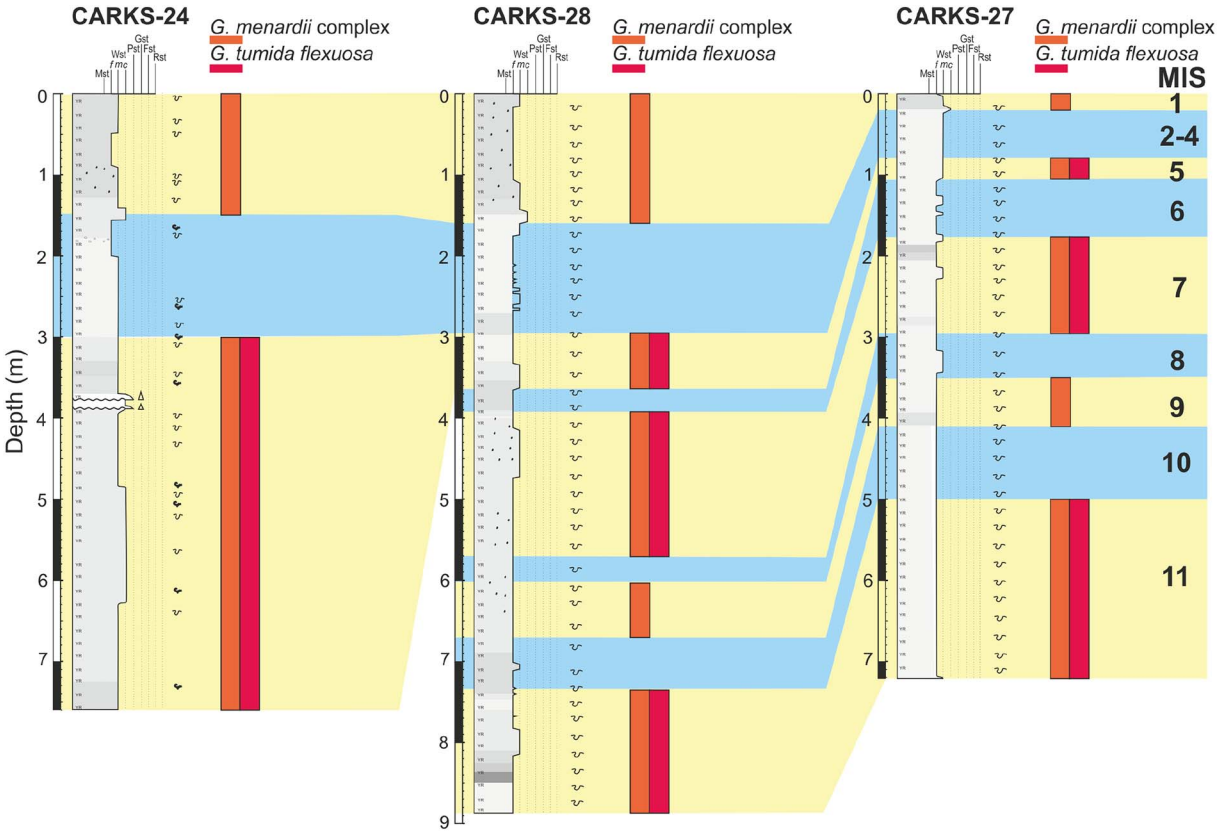

Fig. 9. Lithological description and stratigraphy of Kullenberg cores CARKS-24, CARKS-28 and CARKS-27, which are located in the canyon 4 amphitheatre, canyon 12 terraces and canyon 14 wedge-shaped levees, respectively.

widened part of the canyon (profiles 152 and 146, Fig. 10D).

4.2.3. Canyons with levees and aggrading terraces

This type refers to canyons in an early infill state that are characterised by the development of levees and aggrading terraces (canyons 6 to 16). This morphological type is well illustrated by canyons 10 to 14. They exhibit a linear narrow part along their upper slope with a NNW-SSE-oriented termination, which contrasts with the SSW-NNE orientation of the canyon axes (Fig. 11A and B). Below a water depth of 600 m, these canyons widen considerably and are limited by many arcuate scarps. Canyons 12 and 14 are similar to canyons 3 and 4 in that they have an amphitheatre-shaped central part that is up to 4.5 km wide (Fig. 11A and B).

Because of the lateral coalescence of the canyons, below a water depth of 600 m, the middle slope is not regular and exhibits several eroded interfluve areas. At this depth, a large, 30- to 100-m-high escarpment forms a clear boundary with the steady upper slope. The non-eroded middle slope only appears at the toe-of-slope, where it forms isolated topographic highs (Fig. 11A). The eroded interfluves show several escarpments delimiting large terraces (Fig. 11A). These terraces are subject to significant erosion at the toe-of-slope, along with the development of large angular scarps (Fig. 7 and Fig. 11A).

Terrace geometries are clearly imaged by chirp profiles 148–149, 168 and 170–171 (Fig. 12). These seismic profiles show that terraces are associated with a continuous, layered echo type and are characterised by two types of morphologies.

(1) Terraces can be predominantly aggrading (up to approximately 50 m high); in some places, a restricted “bulge” is present on their edges, as is seen in canyons 11 and 12 (Fig. 12A). The aggrading terraces are not always continuous and can be incised by younger talwegs. This is observed in the eastern terrace of canyon 12, which has been re-incised by canyon 13 (Fig. 12B). The early developmental stage of canyon 13 is evidenced by the incision map, which shows a shallow talweg along its entire length (Fig. 7).
(2) The second type of terrace is characterised by transverse wedge-shaped morphologies that can reach heights of up to 25 m. Based on their wedge shapes and ooze lithologies, these morphologies are interpreted to represent levees built by the overspill of downslope muddy gravity flows bypassing canyon talwegs. The morphologies of these levees are located on both sides of canyon 14, where they are over 2.5 km long (Fig. 12B and C).

The 8.8-m-long CARKS-28 core and the 7.2-m-long CARKS-27 core (Fig. 9) were collected on the western aggrading terraces of canyon 12 and the eastern proximal levees of canyon 14, respectively (Fig. 11A and Fig. 12). These deposits have been dated to the 11 MIS stage (424 ka) (Fig. 9). Both cores are mostly composed of mud to silty wackestone with sedimentation rates during interglacials and glacials of > 10 cm/ka and a few cm/ka, respectively (Chabaud, 2016).

The terraces of canyons 10 to 13 are 3 to 4 times thicker than those of canyon 14 (Fig. 12). The EM302 imagery reveals that low-backscatter deposits are present on the upper slope and spread towards the linear incisions of canyons 10 to 13 (Fig. 11C). In canyon 14, there is no transfer axis that is visible on the reflectivity map; however, some deposits are concentrated around its up-dip linear part (Fig. 11C). Differences in the thicknesses of these terraces are believed to be related to the variability in the transfer of periplatform ooze, which is oriented towards canyons 10 to 13 and reduced towards canyon 14.

4.2.4. Partially and totally filled canyons

Such canyons are partially or completely filled, such as canyons 17 and 18, which are located at the eastern end of the study area. At the eastern edge of our multibeam dataset, these two canyons appear to

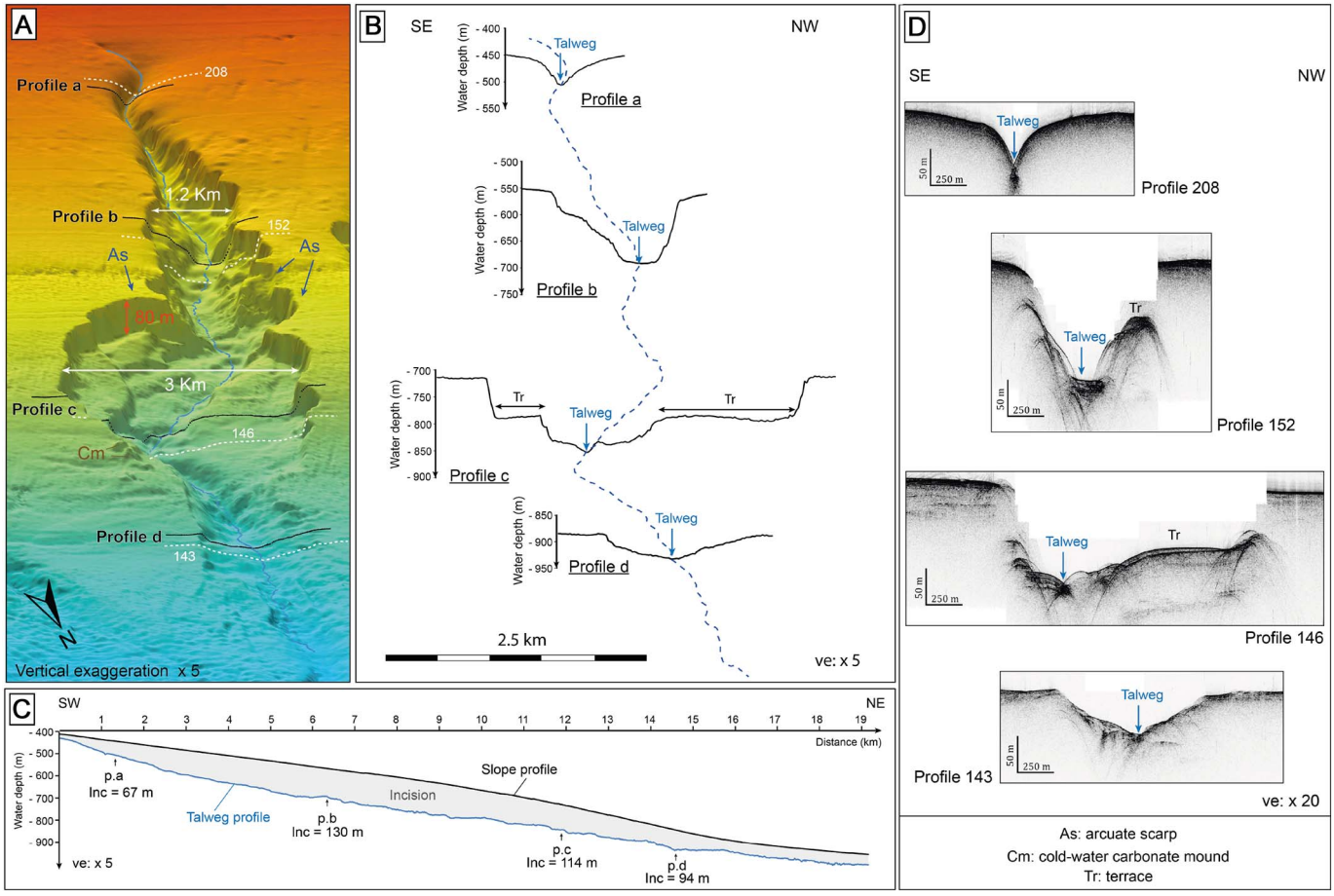

Fig. 10. Detailed characterisation of canyons with up-dip propagating linear incisions (e.g., canyon 5). (A) 3D bathymetrical map of canyon 5 and its associated morphological features. (B) Representative bathymetric cross-sections (noted a to d) along canyon 5, from its up-dip linear incision to its mouth. (C) Comparison of talweg longitudinal profile with interfluve slope profile illustrating incision depth of canyon 5. (D) Chirp seismic profiles 208, 152, 146 and 143 (located in Fig. 6A), showing the along-slope evolution of the internal architecture of canyon 5. Steep edges with several arcuate scarps are clearly imaged. The widened part of the canyon is associated with terraces, but their infill is relatively thin (up to 20 m thick). As: arcuate scarp; Cm: cold-water carbonate mound; Tr: terrace.

merge in the middle slope and are oriented towards the same mouth (Fig. 13A and B). Canyon 18 is composed of a main talweg and two tributary talwegs (18.1 and 18.2). The main talweg is characterised by a U-shape and low incision depth (up to 70 m). In contrast, the talweg of canyon 17 is very steep and can reach depths of up to 130 m. The incision depth map reveals that these two talwegs are not continuous and are partially filled below a water depth of 700 m (Fig. 7).

The chirp profiles 283, 277, 201 and 149–150 display the internal structures of these two canyons (Fig. 13D). In its proximal part, canyon 18 comprises a thick sedimentary unit that is characterised by a continuous layered echo type. This sedimentary unit is up to 100 ms twt thick and is thus approximately 80 m thick (profile 277). The talweg of canyon 18 appears to crosscut this unit throughout its entire thickness, and the tributary axes 18.1 and 18.2 follow and incise the edges of this sedimentary unit. On the EM302 imagery, this infill is associated with homogeneous low backscatter values (Fig. 13C). Up-dip of canyon 18, a thin sedimentary cover with a slightly layered transparent echo type is interpreted to be a muddy apron, similar to the Holocene periplatform ooze wedge seen on the uppermost slope (Rankey and Doolittle, 2012; Mulder et al., *2017*) (profile 283, Fig. 13D). These deposits cover an irregular surface with some incised areas and end with an onlap configuration onto the western side of the canyon. The irregular surface exhibits an indistinct echo type and high backscatter values; therefore; it is interpreted to represent highly indurated ooze deposits (profile 283, Fig. 13D and Fig. 13C).

5. Discussion

5.1. Canyon formation model

The 18 submarine canyons of the northern slope of LBB exhibit significant morphological contrasts and can be classified into 4 types. Their architectural differences indicate the diversity of sedimentary processes involved in submarine canyon formation on this purely carbonate slope. The presence of numerous arcuate slide scarps along the canyon edges strongly implies that retrogressive erosion processes occurred during the early stages of canyon formation (“cutting phase”). On the other hand, the development of levees and aggrading terraces composed of periplatform ooze suggest the overspill of channelised muddy gravity flows and therefore implies that gravity flows produced canyon infills (“filling phase”). In addition, the present-day seafloor shows numerous distributary furrows that are filled by periplatform ooze and oriented towards depositional areas (Figs. 3 and 4), which further supports the presence of small turbidite systems. In this article, we propose a conceptual canyon formation model that highlights the respective effects of erosional and depositional processes on the evolution of canyon morphologies based on our observations.

Due to the presence of numerous scarps on the sides of the 18 described canyons, we propose that slope failures and retrogressive erosion are the main processes involved in canyon initiation. The observation of two contrasting canyon shapes, both with and without linear proximal parts, suggests that retrogressive erosion can be expressed to different degrees during the formation and evolution of a

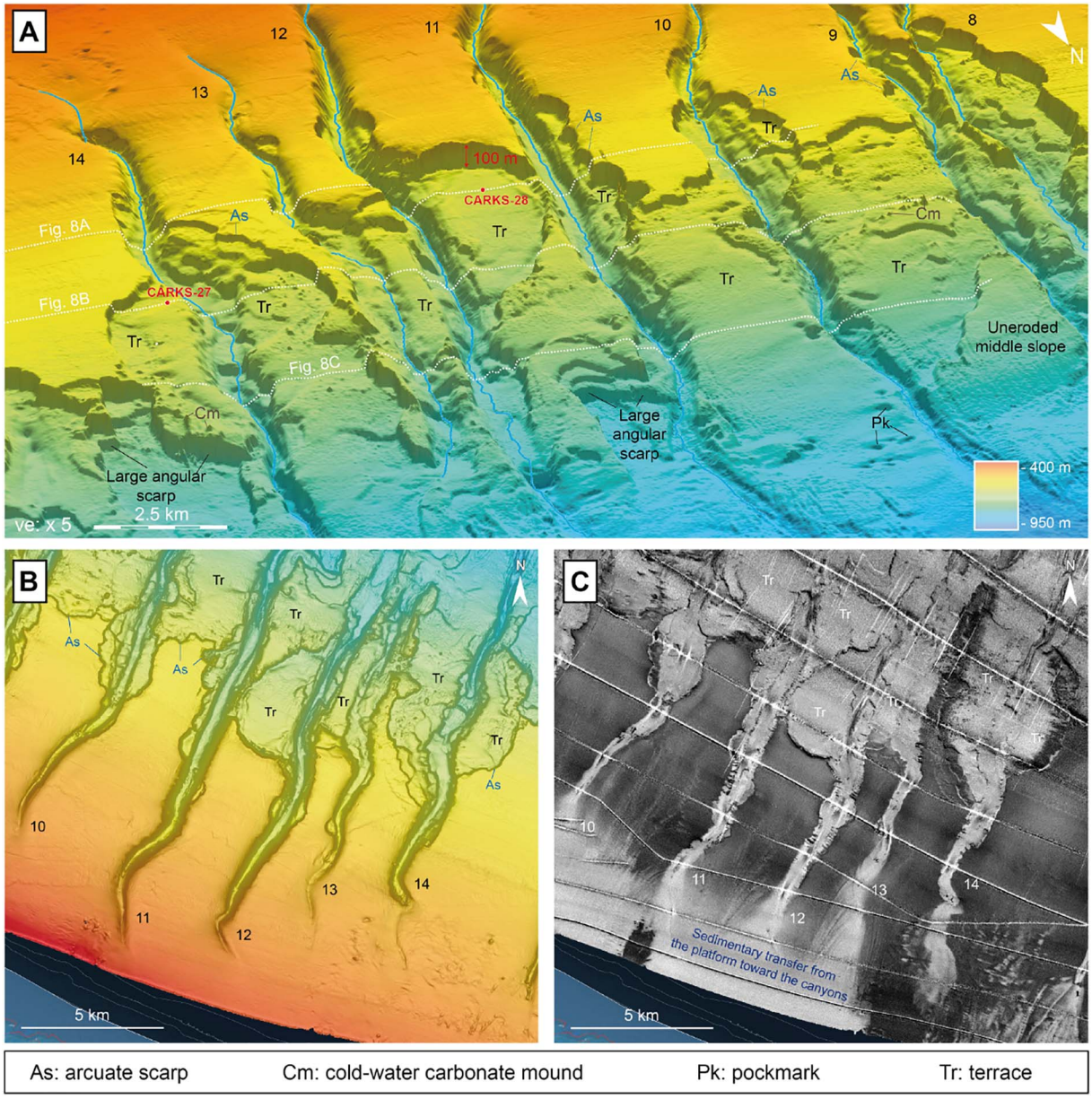

Fig. 11. Detailed characterisation of canyons associated with well-developed aggrading terraces and levees (e.g., canyons 10 to 14). Canyons comprise widened or amphitheatre-shaped parts on the middle slope where thick aggrading terraces and levees have developed and are mainly composed of periplatform ooze (see Fig. 9). Intra-slope erosions occur at the toes of slopes to form large angular scarps. (A) 3D bathymetrical map of canyons 10 to 14 and their associated morphological features. (B) Plan view of bathymetrical map of canyons 10 to 14 and their main morphological features. (C) Plan view of backscatter imagery of canyons 10 to 14. Plan view illustrations show that the extremities of the proximal linear structures are oriented NNW-SSE, i.e., in a different direction than the directions of the axes of the canyons (which are oriented SSW-NNE). Based on their correlation with low backscatter values, these linear incisions are likely sediment transfer axes that would have funnelled periplatform ooze deposits. As: arcuate scarp; Cm: cold-water carbonate mound; Pk: pockmark; Tr: terrace.

canyon. This leads us to propose a logical succession of the first stages of retrogressive erosion processes, similar to those described along the Ribbon Reef canyons on the eastern margin of Australia (Puga-Bernabéu et al., 2011). Finally, based on morphological evidence suggesting the active infill of these canyons, we propose that this retrogressive erosion phase (cutting phase) is followed by a filling phase that is dominated by muddy gravity flows and gravitational settling.

5.1.1. *Intra-slope failures: canyon initiation*

Numerous intra-slope failures have been observed along the LBB slope, such as those seen in the western part of the study area (Sl 1 and Sl 2, Fig. 3A). These affect the slope between water depths of 500 and 800 m and have headscarps that are 30 to 80 m high. At the western end of the northern LBB slope, a larger-scale MTC affects a significant part of the slope above a water depth of 500 m and forms a wide, 44-km-long failure scar (Tournadour et al., 2015). These architectural elements indicate that the LBB slope was affected by numerous slope failures during the Plio-Pleistocene. These initial slope failures were subsequently shaped by retrogressive erosion, bottom currents or downslope gravity flows (Tournadour et al., 2015). We propose that slope failures form the initial stage of submarine canyons and that they are formed by retrogressive erosion from the initial slide scar (Fig. 14).

On carbonate slopes, several parameters can influence intra-slope erosion, such as the sedimentation of underconsolidated periplatform ooze. In the western part of the study area, a downslope evolution in echo type, with better acoustic signal penetration depth at water depths of under 500 m, is seen in the longitudinal chirp profile (Fig. 4A in Chabaud et al., 2016). This suggests that periplatform ooze deposits could be less consolidated along the middle slope, where intra-slope erosion is significant (Fig. 3A) This cementation gradient is interpreted

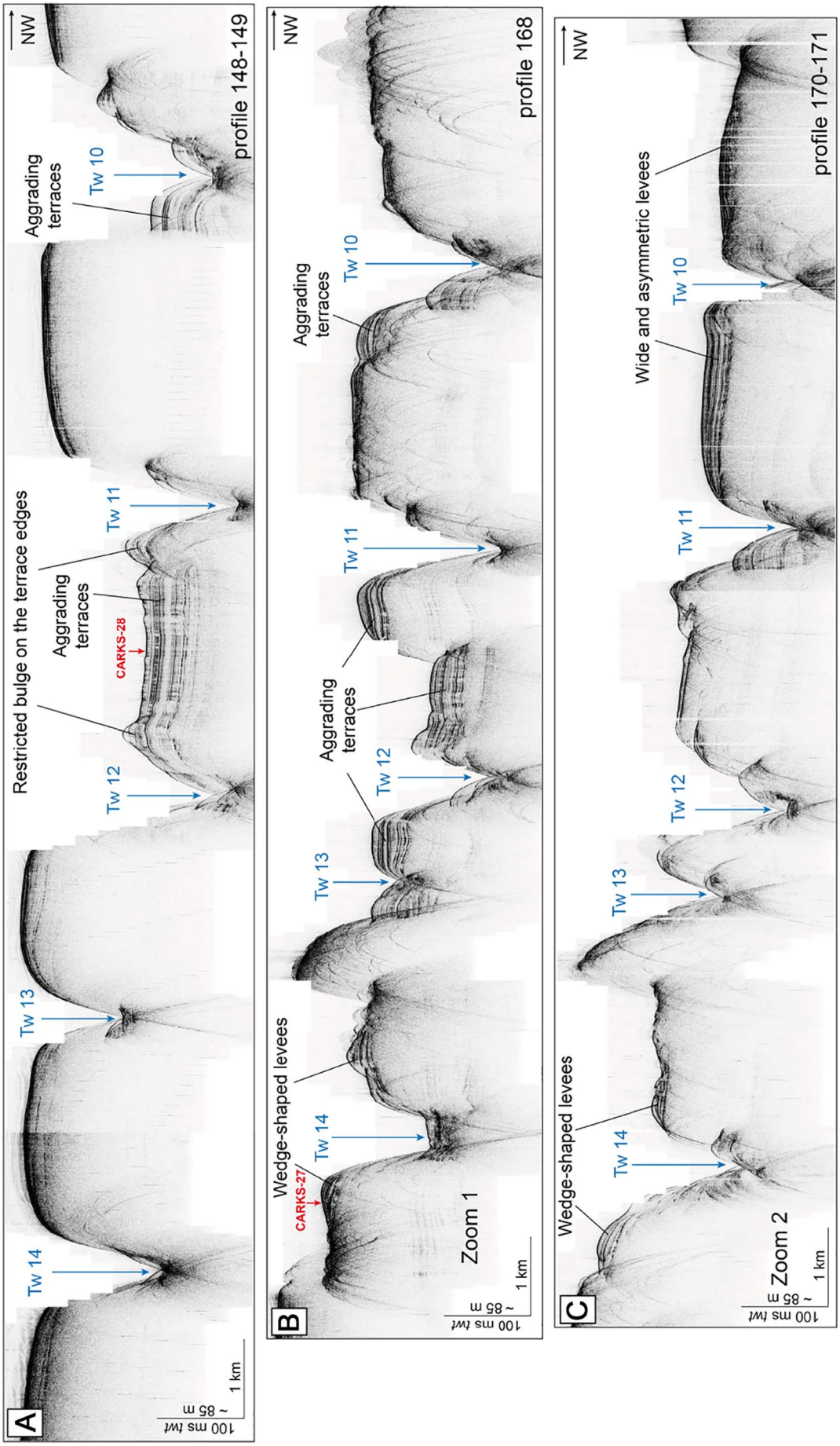

Fig. 12. (A) (B) and (C) representative chirp profiles of canyons 10 to 14 (locations in Fig. 11A), thus illustrating that their internal architectures are characterised by the development of thick aggrading terraces and levees bordering canyon talwegs (Tw). Aggrading terraces can reach thicknesses of 50 m and are typically marked by restricted bulges on their edges. Wedge-shaped levees are seen in the talweg edge of canyon 14 but exhibit less significant thicknesses. Analyses of sediment cores CARKS-27 and 28 reveal that these depositional bedforms are mainly composed of soft, bioturbated periplatform ooze (see Fig. 9).

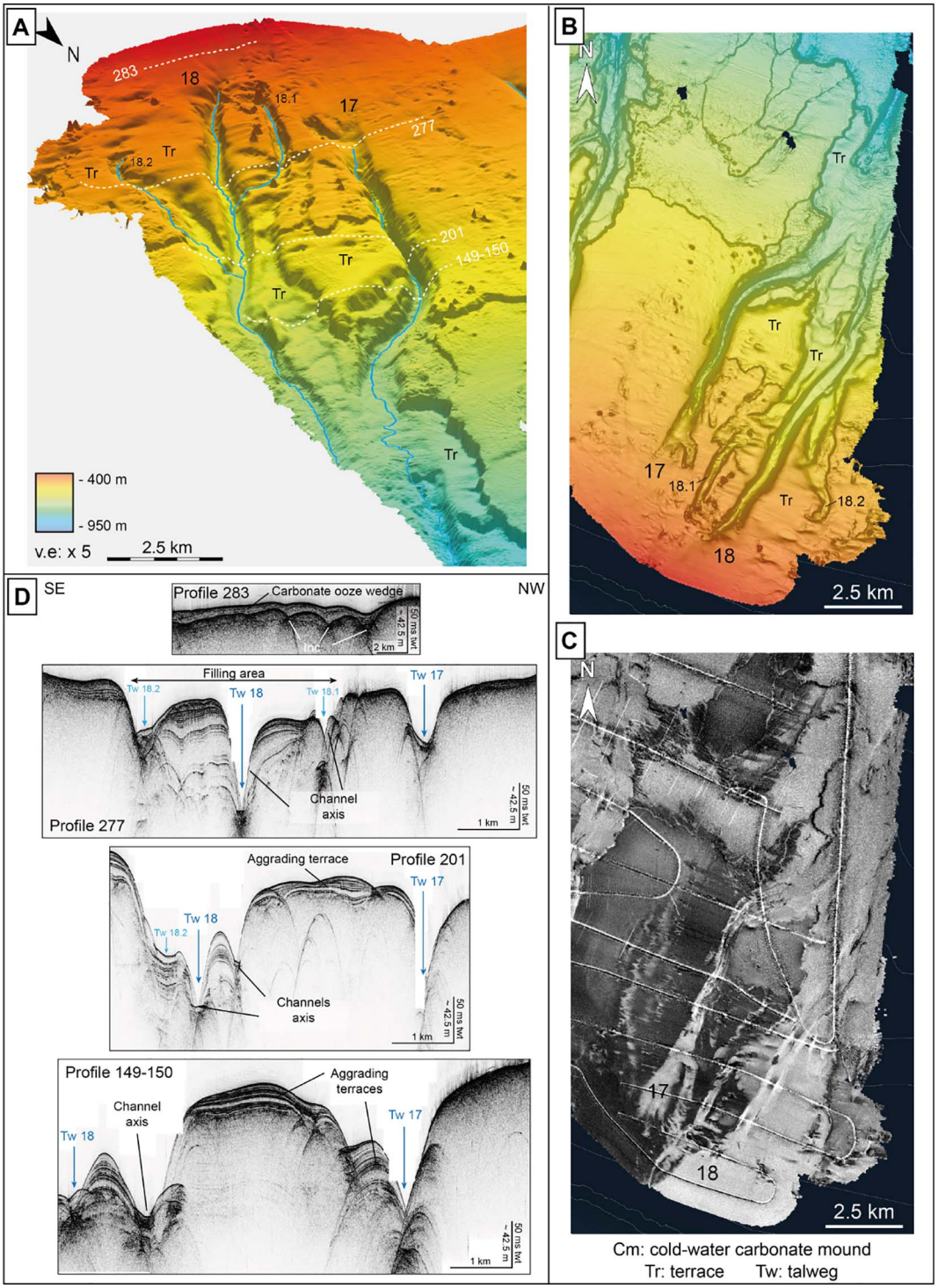

Fig. 13. Detailed characterisation of canyons that are partially or totally filled, e.g., canyons 17 and 18, which comprise an almost totally filled proximal part associated with tributary axes (noted as 18.1 and 18.2). Canyons 17 and 18 tend to converge towards the same mouth. A significant sedimentary infill is present in their proximal part and has been re-incised along the canyon sides by younger tributary axes. (A) 3D bathymetrical map of canyons 17 and 18 and their associated morphological features. (B) Plan view of bathymetrical map of canyons 17 and 18 and their main morphological features. (C) Plan view of backscatter imagery of canyons 17 and 18. (D) Representative chirp profiles of canyons 17 and 18 illustrating their internal architectures, which are notably characterised by partial infill (location in Fig. 13A). Cm: cold-water carbonate mound; Tr: terrace; Tw: talweg.

as the result of the variable diagenetic potential of the periplatform ooze (i.e., high on the upper slope and moderate on the middle slope) combined with the effects of sediment winnowing by bottom currents (Heath and Mullins, 1984; Mullins et al., 1984; Tournadour, 2015; Chabaud et al., 2016).

5.1.2. Retrogressive erosion continuation: canyon formation

The observed morphological contrast between canyons with an up-dip linear incision above a water depth of 600 m and canyons with a widened part or an amphitheatre shape under a water depth of 600 m could be the result of a decrease in the intensity of retrogressive erosion due to an upslope increase in the diagenetic induration of the carbonate ooze and/or the decrease in the slope gradient from 2.5° to 1.5° above a

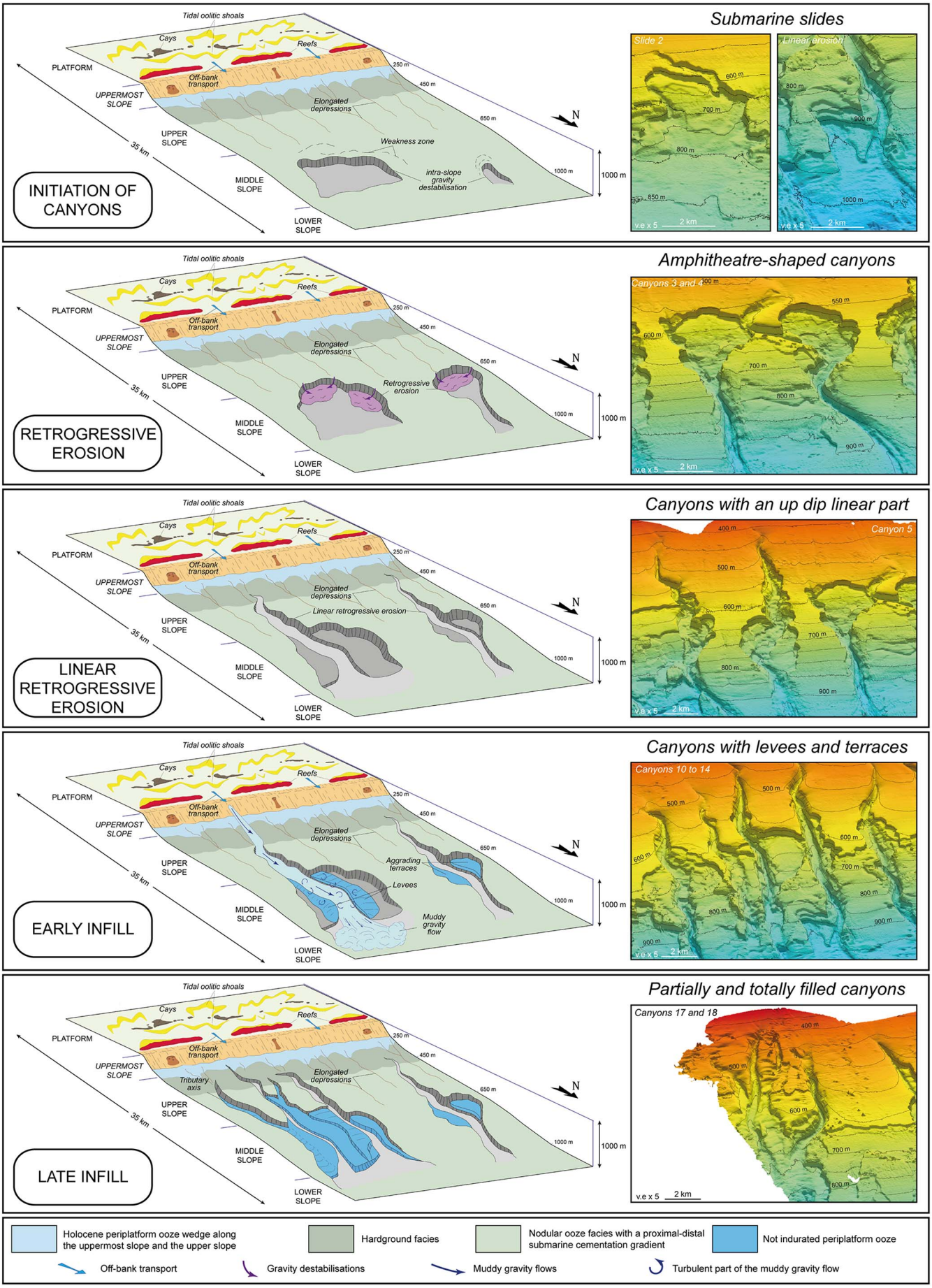

(caption on next page)

Fig. 14. Theoretical model for LBB canyon formation and evolution from canyon initiation to infill. Based on our morphological classification, this model comprises five evolutionary stages, each of which is illustrated by a representative morphological example. Canyon initiation is thought to essentially result from slope failures occurring on the middle slope. Following this, canyons propagate up-slope due to two successive phases of stepped retrogressive erosion controlled by a submarine cementation gradient that decreases downslope. The first phase of retrogressive erosion leads to the widening of canyons up to a water depth of 600 m, whereas the second phase forms linear incisions up to a water depth of 450 m, where it is stopped by a sedimentary facies transition between a nodular ooze facies and a hardground facies. Subsequently, after this mostly erosional phase, muddy gravity flows are responsible for canyon infill, which is associated with the formation of aggrading terraces and levees. This infill phase eventually leads to the onset of the final blanketing of the canyon, marking the end of the "erosion-fill" cycle.

water depth of 600 m (Fig. 3B).

Canyons 3 and 4, for instance, lack up-dip linear incisions and show an amphitheatre shape that stops at a water depth of 550 m. The numerous arcuate scarps along their edges suggest that they initially formed by retrogressive erosion along a single narrow linear incision that extends considerably upslope to form proximal amphitheatre-shaped parts (Fig. 8). These amphitheatre-shaped parts also characterise canyons 12 and 14. The amphitheatre-shaped canyons are interpreted to have formed during a logical succession of retrogressive erosion processes (Fig. 14). During this stage, retrogressive erosion stopped at a water depth of approximately 550–600 m to form a deep morphological limit that can be observed throughout the entire study area. From canyon 6 to 18, this boundary is evidenced by a continuous escarpment that is up to 100 m high. As this feature was previously seen in the subbottom profiler dataset (Fig. 4A in Chabaud et al., 2016 and Fig. 5 in this contribution), we propose that this first morphological limit is related to the submarine cementation gradient, which could imply a change in the transitional up-dip facies from a non-indurated periplatform ooze towards a nodular ooze facies. Unfortunately, in the eastern part of the study area, the middle slope is rarely preserved and no core data are available with which to confirm this hypothesis. The presence of this potential diagenetic front could explain the decrease in retrogressive erosion processes observed along the upper slope. This diagenetic front could cause failures to form on the sides of the canyons rather than on the upslope part. Consequently, the canyon could become enlarged and form the amphitheatre-shaped feature.

In contrast, all canyons except for canyons 3 and 4 are characterised by an up-dip narrow linear incision between water depths of 450 m and 600 m. Once more, the occurrence of numerous scarps on the sides of these linear parts suggests that they are mainly formed by retrogressive erosion. Similar to the previous phase, these again involve retrogressive erosion progresses; however, these follow a different pattern. At water depths that are shallower than 600 m, canyons still expand upslope but only form narrow linear incisions, probably because the proximal carbonate deposits are more cemented, thus increasing the shear resistance of carbonate sediments and the stability of the canyon edges (Fig. 14). Thus, canyons tend to incise rather than to enlarge, leading to the more pronounced entrenchment of incisions. The low penetration echo-type observed from 350 to 600 m on the subbottom profiler (Fig. 5) supports this hypothesis. In this part, the subbottom profiler is calibrated at a water depth of 600 m by the CARKS-26 core, in which a nodular ooze facies indicates the existence of submarine diagenetic processes. The retrogressive erosion stage stops at a water depth of approximately 450 m, thus forming a second main morphological limit where canyons definitely end. Similar to the first morphological limit, the end of the retrogressive erosion stage is interpreted to represent the result of a downslope facies transition from a hardground facies towards a nodular ooze facies, as is suggested by the subbottom profiler dataset, in which there is an acoustic facies change from an indistinct echo type towards a discontinuous layered echo type at a water depth of approximately 500 m (Fig. 5A).

Most of the canyons exhibit a V-shape. According to Jobe et al. (2011), this is typical of canyons related to hyperpycnal flows that are directly linked with a river mouth. This interpretation is not consistent with our environmental setting. In the LBB case study, the V-shape is controlled by the retrogressive erosion that sometimes affects very cemented material. Over time, canyons evolve from being V-shaped to being U-shaped because their filling is controlled by depositional processes involving fine-grained sediment without significant erosion.

In other case studies, it has been proposed that downslope eroding gravity flows could be combined with retrogressive erosion to form submarine canyons (e.g., Pratson et al., 1994; Pratson and Coakley, 1996). Indeed, the local topography created following intra-slope destabilisations can funnel the sediment fluxes coming from the platform and increase the incision of the slope if the flow capacity is high enough. In our study, several shallow linear depressions defined as S.1 (Fig. 8A, B and C) are observed on the upper slope (Fig. 14), which could potentially imply that downslope gravity flows occurred during this stage of canyon formation. However, these morphologies are widespread on the upper slope and are thus not systematically connected with the proximal parts of the canyon. Therefore, their origin is likely independent of the formation of the canyon. That said, these shallow linear depressions strongly suggest that the off-bank transport of active downslope periplatform ooze will ultimately contribute to the canyon infills. As these shallow linear depressions are present along the entire toe of the prograding wedge, they could also result from local small-size avalanching that is initiated along the steepest part of this wedge.

In the Ribbon Reef Canyons on the eastern margin of Australia (Puga-Bernabéu et al., 2011), which represents the only similar case study that is currently comparable with the LBB canyons, it is notable that retrogressive erosion propagates up to the platform edge until it is fully blocked by reefs. This difference is likely linked to the steepness of the slope of the Australian margin (which ranges from 7° to 15°) compared to the gentler LBB slope (which ranges from 1.5° to 2.5°).

5.1.3. Canyon infill by periplatform ooze

Canyons 10 to 14 are bordered by aggrading terraces that are typically associated with wedge-shaped levees (Figs. 11 and 12). These morphologies are composed of not indurated, bioturbated periplatform ooze with a mud to silty wackestone texture (CARKS-27 and 28 Fig. 9, located in Figs. 11A and 12).

The off-bank transport from the platform towards the canyons was recently characterised on the uppermost slope (at a water depth of > 300 m) by Mulder et al. (2017). These authors showed the presence of shallow tidal channels connected to linear incisions of submarine canyons that directly feed these canyons with platform-derived sediments, thus forming low-density currents. The transported sediments mostly consist of periplatform ooze, thus suggesting that these flows transport platform sediments mixed with fall-out sediments that can be incorporated during transport. Canyon terraces and levees appear to mainly comprise by the overbank of the dilute upper parts of these flows, which are therefore partly confined within the canyon talweg (Fig. 14). Canyon 13 was developed by the incision of the eastern terrace of canyon 12 (Figs. 11 and 12). These morphological features suggest that a new canyon can be formed by the subsequent bypassing of muddy gravity flows across a previous deposited muddy infill.

Canyons 17 and 18 are characterised by the presence of a distributary axis connected with the up-dip linear parts of canyons. This proximal domain is largely filled by periplatform ooze (Fig. 13). These canyons are interpreted to be the result of the advanced filling stage where new tributary axes develop within the proximal part of the canyon (Fig. 14); this points to the intensification of the sediment fluxes that are funnelled within the canyons. Of particular interest in canyons 17 and 18 is that the orientations of these canyons differ from those that are located approximately 10° to the east. Moreover, they have the

same orientation as tidal passes associated with oolitic shoals to the east of Carter's Cay (Figs. 6A and 7). This leads us to suggest that the proximal parts of canyons are located in front of a major transfer axis of periplatform ooze, which could explain their current advanced degree of infill (Fig. 13).

The distributary furrows suggest that the by-pass of sediment fluxes along the lower slope from the canyon mouths towards the three distal depositional areas (Fig. 4A and C). The low backscatter that characterises the shallow distributary furrows suggests that they are filled by fine-grained or not indurated sediments and could be thus formed by cut and fill processes. Along with such downslope sediment transfers, the linear structures seen on the acoustic imagery ranging from N°300 to N°270 (Fig. 4B) attest to the role that bottom currents play in the sedimentary dynamics occurring in the eastern part of the study area. The SE-NW-flowing Antilles Current could have enough capacity to form these linear structures and therefore trap some of the fine-grained sediments originating from muddy gravity flows at the canyon mouths. Then, these deep sea bank-derived sediments could participate in the LBB drift growth (Tournadour et al., 2015; Chabaud et al., 2016). Another hypothesis is that linear morphologies are the result of the deepest circulation of the Labrador Sea Water, which could transport sediments towards the deep basin.

The trapping of sediment by bottom currents could explain the relatively reduced sediment rates on the lower slope during the Plio-Pleistocene (33 m/m.y. at ODP site 628 and 14–15 m/m.y. at ODP site 627) compared to the middle slope (62 m/m.y. at ODP site 630 (Austin et al., 1986)) despite the architectural evidence of the downslope by-pass.

The lack of such a filling stage in the active canyons of the Australian Great Barrier Reef margin is another stark difference with the LBB canyons. This discrepancy could be explained by the steepness of the Australian slope, which could induce a dominantly erosional process and potentially completely bypass sediments in transit in the canyons. In addition, a less productive “carbonate factory” on the eastern Australian margin than on LBB could also explain its weaker off-bank transport and thus the availability of fewer sediments to fill the canyons.

5.2. Control parameters on canyon evolution along the LBB slope

The proposed theoretical model of the evolution of the canyon, from initiation to infill, is characterised by the specific sedimentary processes and architectures summarised in Fig. 15. These include three main stages of evolution occurring at three different time periods: (1) initiation caused by intra-slope destabilisations, (2) up-slope migration by retrogressive erosion, and (3) canyon infill by periplatform ooze. Here, we address the potential control parameters for each of these three time periods.

(1) This dataset suggests that canyon initiation results from slope failures. Several submarine slides have been observed along the middle slope of LBB; these show numerous arcuate scarps on their steep edges, thus suggesting a *continuum* to canyon formation through retrogressive erosion processes. Large submarine slides frequently occurred along the accretionary Bahamian slopes during particular periods of the Neogene (Austin et al., 1988; Schlager et al., 1988; Jo et al., 2015; Principaud et al., 2015; Tournadour et al., 2015), but correspond to various triggering mechanisms. Slope failures could have been triggered by high sedimentation rates, the intensification of bottom currents or earthquakes.
   - The LBB submarine canyons appear to have formed during a period of high slope aggradation linked to high carbonate production on the platform in the Pliocene (Austin et al., 1988; Harwood and Towers, 1988; McNeill et al., 1998; Tournadour, 2015). Submarine landslides could therefore have been triggered by sediment overloading.
   - The northern slope of LBB is strongly influenced by the SE-NW-flowing Antilles Current (Tournadour et al., 2015; Chabaud, 2016). The intensification of the Antilles current could have enhanced the shear stress on the middle slope and favoured the triggering of slides.
   - Earthquakes can be another triggering mechanism for large slides along the slope. Indeed, Jo et al. (2015) attributed the margin collapse of the southwestern margin of GBB to the tectonic activity in the vicinity of the Cuban fold and thrust belt. Although the northern slope of LBB is located relatively far from the Cuban fold and thrust belt, several studies have interpreted several normal faults or tectonic tilts as being related to the Cuban orogenesis (Mullins et Van Buren, 1981; Van Buren and Mullins, 1983; Mulder et al., 2012b).

In addition to these triggering parameters, preconditioning factors could also favour slope failures. Indeed, submarine landslides could be linked to the presence of cemented surfaces generated by early diagenesis, which typically occurs during lowstand periods (Malone et al., 2001). These well-lithified surfaces could form a preferential detachment horizon and a gliding plane for the sliding sediments. For example, along the western slope of GBB, Principaud et al. (2016) identified the Late Messinian–Early Pliocene horizon as a common detachment surface of the Plio-Pleistocene MTCs. Moreover, Harwood and Towers (1988) identified numerous detachment surfaces along the LBB slope in the Pliocene-Holocene interval that likely controlled large-scale rotational movements and slumped masses (Fig. 2B).

(2) The up-slope migration by retrogressive erosion includes two conceptual steps that control the morphological contrasts between the amphitheatre shapes at water depths ranging from 650 m to 800 m and the linear V-shaped incisions at water depths ranging from 450 m to 600 m. These two backstepping stages could be diachronous or coeval to the initiation of the canyon due to slope failures. In this case study, it is not possible to determine the relative timing of these steps. Moreover, our dataset does not allow us to identify any preferential period for the formation of V-shaped incisions (e.g., lowstand vs highstand periods). However, V-shaped incisions have been identified on the western slope of GBB, which have been dated to the Messinian and Early Pliocene and are associated with a relative sea level drop (Anselmetti et al., 2000; Principaud et al., 2016). In addition, Wunsch et al. (2017) interpreted that the triggering of failures occurred on the leeward slope of the GBB during the last sea-level fall.

The triggering mechanisms of such retrogressive erosions have been attributed to downslope eroding gravity flows in many other case studies (Pratson and Coakley, 1996). However, in this context, it remains difficult to distinguish between gravity-driven intra-slope erosion and downslope erosion caused by gravity flows that were initiated from the platform edge during canyon formation. That said, in this purely carbonate setting, it seems unlikely that gravity flows generated at the platform edge would have had sufficient intensity to cause seaward excavation.

(3) Under the current highstand shedding settings, carbonate production on the platform is believed to be maximal and the intensity of platform-derived sediment fluxes is expected to increase moving towards deep sea environments (Droxler and Schlager, 1985; Grammer and Ginsburg, 1992; Schlager et al., 1994; Jorry et al., 2010). However, the transfer of periplatform ooze is not uniform along the slope, i.e., significant alongshore variability must be considered when dealing with platform-basin sediment transfer. On LBB, the latter is significant on the leeward western platform margin, where there are no barrier reefs, but it progressively decreases towards the windward eastern margin, which is associated

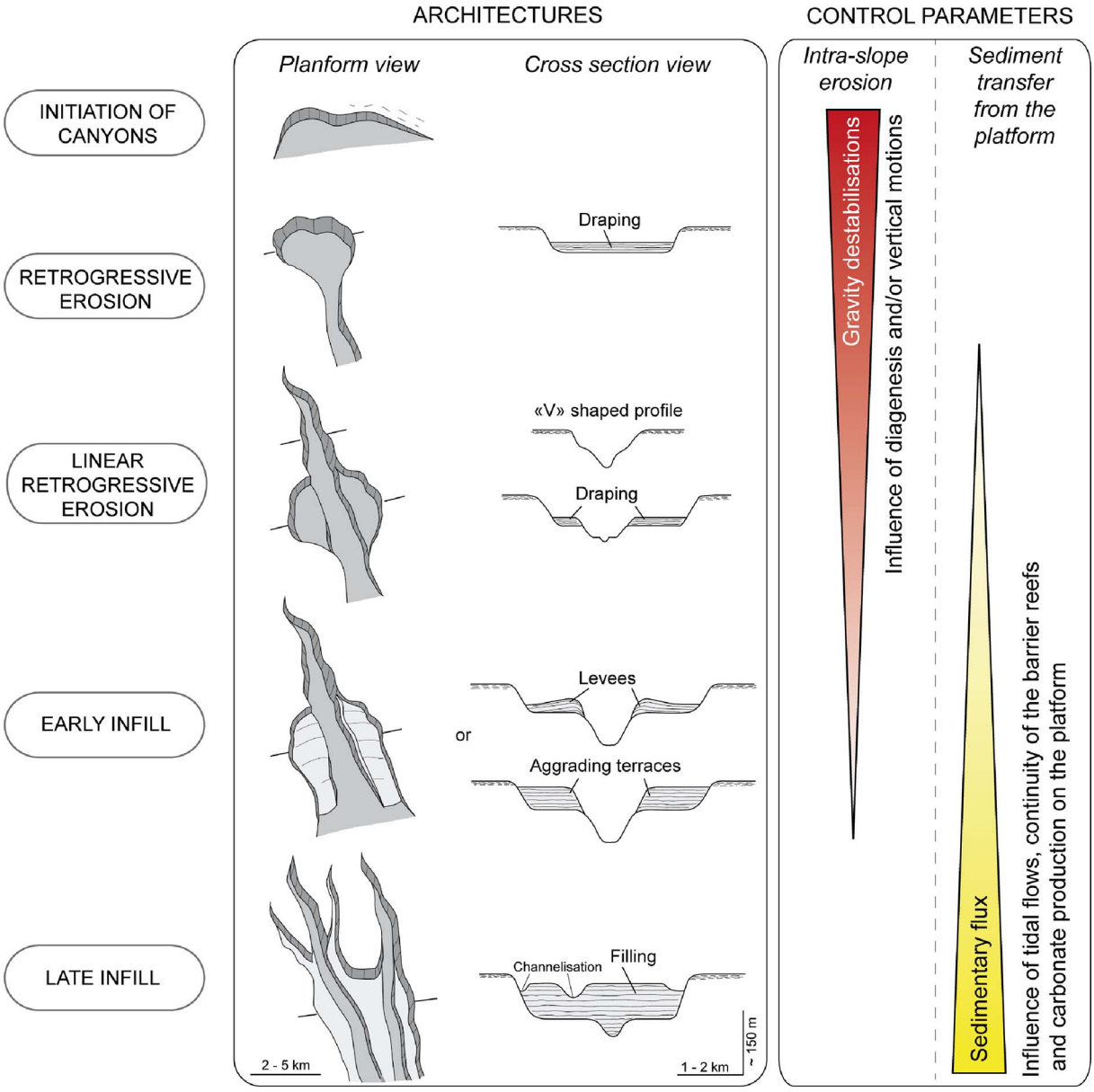

Fig. 15. Summary diagram illustrating the platform morphologies and associated architectural styles of LBB canyons relative to their main control parameters (i.e., gravity destabilisations and sediment fluxes).

with discontinuous barrier reefs (Fig. 3A). Periplatform ooze is believed to be transported by either density cascading or muddy gravity flows confined within canyons. Present sea level highstand conditions have led to the flooding of the platform (between 3 and 8 m) but remains lesser than that recorded during earlier interglacials, such as MIS5e. During this latter extreme highstand, the complete flooding of the platform generated the full activity of the carbonate factory and increased carbonate production and off-bank transport (Chabaud et al., 2016; Chabaud, 2016). The presence of confined turbidite levees suggests that muddy flows may play an important role in canyon differentiation during the filling stages. The intensification of canyon infill may be linked to the development of preferential transfer axes for muddy gravity flows, particularly when the sea level is higher than the present sea level (Chabaud, 2016). The carbonate exports can also supply a highstand wedge, such as the Holocene wedge, along the uppermost slope of LBB (Rankey and Doolittle, 2012). The export processes of the periplatform ooze appear to be linked to the tidal dynamics located near the passes and, to some extent, towards canyons (Mulder et al., 2017). In addition, the Antilles current or/and the Labrador Sea Water, which circulate along the LBB slope, can also limit the infill of the submarine canyons by reworking fine-grained sediments, in addition to increasing carbonate cementation.

5.3. Comparison with other submarine canyons of the Bahamian slopes

The Bahamian slopes are characterised by several downslope by-pass features indicating the transfer of sediments from platforms towards deep basins (Table 1). In this comparison, we only consider canyons that are located between water depths of 0 to 1000 m (referred to as “accretion” sensu Schlager and Ginsburg, 1981), in contrast to those that are located along the U.S. East Coast continental margin, which are located at water depths ranging from 2000 to 4000 m (referred to as “erosion” sensu Schlager and Ginsburg, 1981), such as the Great Abaco Canyon and the San Salvador Canyon (Mullins et al., 1982; Ravenne et al., 1985).

The downslope by-pass architectures have been described (that are 50 to 200 m deep) on the southern slope of LBB by Burns and Neumann

Table 1
Synthesis of the morphologies and process interpretations of presently known downslope by-pass architectures along the Bahamian slopes (up to 1000 m water depth).

Localisation	Type	Water depth	Incision depth	Description	Interpretation	References
Northern slope of Little Bahama Bank (LBB)	Canyons	From 450 to 1000 m	100 to 150 m	Canyons with an up-dip linear incision and an amphitheatre-shaped head.	Canyon formation mainly controlled by retrogressive erosion.	-Mulder et al., 2012b -This study
Southern slope of Little Bahama Bank (LBB)	Inactive canyons		10 to 200 m		Interpreted as erosional features created by turbidity currents and other gravity-driven sediment flows. Occur sporadically.	-Burns and Neumann, 1987
Western slope of Great Bahama Bank (GBB)	Buried canyons		0.05 to 0.15 s twt	V-shaped incisions observed on 2D seismic profiles	Interpreted as being related to a relative sea-level fall.	-Anselmetti et al., 2000 -Principaud et al., 2016
Western slope of Great Bahama Bank (GBB)	Seafloor gullies	From 400 to 700 m	10 to 20 m	Seafloor gullies, generally associated with sediment waves.	Interpreted as structures linked to density cascading processes, mostly during relative sea-level highstands.	-Wilson and Roberts, 1992, Wilson and Roberts, 1995 -Mulder et al., 2012a -Betzler et al., 2014 -Wunsch et al., 2017
East windward slope of Cay Sal Bank (CSB)	Channels	From 300 to 700 m	10 to 60 m	Channels characterised by a dentritic pattern at their upslope end.	Formed by turbidity currents induced by surface currents during relative sea-level lowstands.	-Wunsch et al., 2017

(1987). These were studied using only chirp profiles and their detailed geometries are still poorly known; thus, we cannot comprehensively compare them to the canyons described in this paper. Other canyons have been identified on the western slope of GBB as V-shaped incisions using 2D seismic profiles; these were interpreted as being related to relative sea-level falls during the Messinian and the Pliocene without specifying any formation processes (sequence f in Anselmetti et al., 2000; Me and PL-1 surfaces in Principaud et al., 2016). These incisions, which are 0.05 to 0.15 s twt deep, are currently completely filled. A second type of downslope by-pass geometries, called “gullies”, have been very well-imaged on the present-day sea floor of the western slope of GBB (Mulder et al., 2012a; Betzler et al., 2014; Wunsch et al., 2017). These incisions are located on the slope at water depths between 400 m and 700 m, are 10 to 20 m deep and are generally associated with sediment waves. They have been interpreted as structures related to density cascading processes (Wilson and Roberts, 1992, 1995), which are believed to be most active during relative sea level highstands, when carbonate production is maximal (Betzler et al., 2014; Wunsch et al., 2017). In addition, on the east windward slope of Cay Sal Bank (CSB), several channels are present on the seafloor at water depths ranging from 300 to 700 m, with incisions at depths of 10 to 60 m; these channels are characterised by dendritic patterns at their upslope ends (Wunsch et al., 2017). The authors proposed that channels on this windward slope have been formed by turbidity currents induced by surface currents during relative sea-level lowstands.

Compared to all of these features, canyons on the northern slope of LBB exhibit very atypical shapes; very few, if any, morphologies are similar to those of the other present-day Bahamian slopes. However, despite their atypical shapes, their dimensions are comparable to those of the buried canyons (i.e., V-shaped incisions) observed on the western slope of GBB and the channels on the windward slope of CSB (Table 1). The latter are interpreted to have been formed during lowstand periods with increased sediment fluxes coming from the platform. According to these authors, the associated gravity flows could have been strong enough to erode the slope and produce submarine canyons (Wunsch et al., 2017). In our case study, downslope gravity flow erosion has not yet been ruled out as a cause of canyon formation, but it appears unlikely that gravity flows alone could generate incisions that are > 100 m deep. Moreover, the numerous slide scars on the edges of canyons represent compelling evidence for the role of retrogressive erosion processes in canyon formation. Therefore, we consider that muddy gravity flows play a larger role in the infill of canyons than in their initial formation.

6. Conclusions

The submarine canyons on the northern slope of LBB constitute a unique case study that can be used to improve our understanding of canyon formation in purely carbonate settings. Using a very high-resolution dataset, we are able to provide new constraints on the morphologies, evolution and initiation of the LBB northern slope canyons. This allows us to discuss their control parameters.

Canyons can been classified as one of four morphological types: canyons ending with an amphitheatre-shaped part (1); canyons expanding upslope by deep linear incisions (2); canyons associated with aggrading terraces and levees (3); and canyons that are partially or completely filled (4). Due to progressive filling, the transversal profiles of canyons progressively evolve from being V-shaped to being U-shaped. Based on these main morphologies, their distributions on slopes and their internal architecture, we propose a detailed model for the formation and evolution of carbonate slope canyons. Canyons are believed to be initiated by slope failures that propagate upslope due to two successive stages of retrogressive erosion. The first retrogressive erosion stage produces the widened shape or amphitheatre shape of canyons that progress up-slope up to water depths of 600 m. The second stage of retrogressive erosion leads to the formation of linear incisions up to water depths of 450 m. Then, the filling of canyons by muddy gravity flows and gravitational settling forms aggrading terraces and wedge-shaped levees. This filling process eventually leads to the onset of canyon blanketing.

The present canyon morphology is a result of cut and fill phases. This model therefore suggests that canyon formation in such settings is essentially controlled by retrogressive erosion processes, as is evidenced by the numerous arcuate scarps located on the sides of the canyon. This study demonstrates the key role that carbonate lithology plays in canyon evolutions that are driven by retrogressive erosion. Indeed, we show that a downslope gradient of submarine cementation controls retrogressive erosion patterns, which induce very specific morphological contrasts between LBB canyons. Canyon infill, which is dominated by periplatform ooze, represents the result of pelagic sedimentation combined with the deposition of sediments by non-erosive muddy gravity flows initiated from the platform edge, as is suggested by the presence of wedge-shaped levees and confined aggrading terraces within canyons. Filling by periplatform ooze and fine-grained turbidite probably occur during different highstand periods, depending of the height of the water flooding the platform and the related productivity of the carbonate factory. Available sediments involved in the canyon infills are thus mainly controlled by the production of the carbonate

platform. However, the spatial distribution of the platform-derived sediment fluxes is not uniform along the slope. There is indeed a strong alongshore variability in off-bank transport that is closely linked with the orientation of the platform with respect to wind direction and oceanic current circulation and the relative continuity of the reef barrier. Sedimentary fluxes are dominant in the leeward western platform margin, which contains no barrier reefs; these fluxes progressively decrease moving towards the windward eastern margin, which is associated with discontinuous barrier reefs. In addition, variations are also caused by the remobilisation of fine particles by the surface Antilles current heading towards the northwestern part of the LBB slope and/or the bottom Labrador Current heading towards the southeastern part of the LBB slope. Therefore, the preservation of LBB canyons since the Pliocene could be the result of relatively low sedimentation rates along their windward margins and/or the result of the by-pass of platform-derived sediment flows in the canyon talweg towards the deep basin.

Akcnowledgements

We thank the captain and the crew of the R/V Le Suroît for the quality of the data acquired during the Carambar cruise 1. We acknowledge TOTAL for their support and their scientific contribution to this project. We also thank to two anonymous reviewers for their comments and suggestions which improved the early version of this manuscript.

References

Anselmetti, F.S., Eberli, G.P., Ding, Z.-D., 2000. From the Great Bahama Bank into the Straits of Florida: a margin architecture controlled by sea-level fluctuations and ocean currents. Geol. Soc. Am. Bull. 112, 829–844.

Austin, J.A., Schlager, W., Palmer, A.A., Comet, P.A., Droxler, A., Eberli, G.P., Fourcade, E., Freeman-Lynde, R., Fulthorpe, C.S., Harwood, G., Kuhn, G., Lavoie, D., Leckie, M., Melillo, A.J., Moore, A., Mullins, H.T., Ravenne, C., Sager, W.W., Swart, P., Verbeek, J.W., Watkins, D.K., Williams, C., 1986. Proc. ODP Initial Report. vol. 101.

Austin, J.A., Schlager, W., Palmer, A.A., Comet, P.A., Droxler, A., Eberli, G.P., Fourcade, E., Freeman-Lynde, R., Fulthorpe, C.S., Harwood, G., Kuhn, G., Lavoie, D., Leckie, M., Melillo, A.J., Moore, A., Mullins, H.T., Ravenne, C., Sager, W.W., Swart, P., Verbeek, J.W., Watkins, D.K., Williams, C., 1988. Proc. Scientific Results. vol. 101.

Ball, M.M., 1967. Carbonate sand bodies of Florida and the Bahamas. J. Sediment. Res. 37, 556–591.

Benson, W.E., Sheridan, R.E., Pastouret, L., Enos, P., Freeman, T., Murdmaa, I.O., Worstell, P., Gradstein, F., Schmidt, R.R., Weaver, F.M., Stuermer, D.H., 1975. Initial Reports of the Deep Sea Drilling Project. vol. XLIV (Leg 44).

Betzler, C., Lindhorst, S., Eberli, G.P., Lüdmann, T., Möbius, J., Ludwig, J., Schutter, I., Wunsch, M., Reijmer, J.J.G., Hübscher, C., 2014. Periplatform drift: the combined result of contour current and off-bank transport along carbonate platforms. Geology 42, 871–874.

Bliefnick, D.M., Robertson, A.H.F., Sheridan, R.E., 1983. Deposition and provenance of Miocene intraclastic chalks, Blake-Bahama Basin, western North Atlantic. In: Initial Reports DSDP, Leg 76, Norfolk to Fort Lauderdale, pp. 727–748.

Burns, S.J., Neumann, A.C., 1987. Pelagic sedimentation on an inactive gullied slope, northwest providence channel, Bahamas. Mar. Geol. 277–286.

Canals, M., Puig, P., de Madron, X.D., Heussner, S., Palanques, A., Fabres, J., 2006. Flushing submarine canyons. Nature 444, 354–357.

Chabaud, L., 2016. Modèle stratigraphique et processus sédimentaires au Quaternaire sur deux pentes carbonatées des Bahamas (leeward et windward). Université de Bordeaux.

Chabaud, L., Ducassou, E., Tournadour, E., Mulder, T., Reijmer, J.J.G., Conesa, G., Giraudeau, J., Hanquiez, V., Borgomano, J., Ross, L., 2016. Sedimentary processes determining the modern carbonate periplatform drift of Little Bahama Bank. Mar. Geol. 378, 213–229.

Chérubin, L.M., 2014. High-resolution simulation of the circulation in the Bahamas and Turks and Caicos Archipelagos. Prog. Oceanogr. 127, 21–46.

Damuth, J.E., Hayes, D.E., 1977. Echo character of the East Brazilian continental margin and its relationship to sedimentary processes. Mar. Geol. 24, 73–95.

Droxler, A.W., Schlager, W., 1985. Glacial versus interglacial sedimentation rates and turbidite frequency in the Bahamas. Geology 13, 799–802.

Enos, P., 1974. Surface Sediment Facies Map of the Florida–Bahamas Plateau. Geological Society of America (Map 5).

Ericson, D.B., Wollin, G., 1956. Micropaleontological and isotopic determinations of Pleistocene climates. Micropaleontology 2, 257–270.

Ericson, D.B., Ewing, M., Wollin, G., Heezen, B.C., 1961. Atlantic deep-sea sediment cores. Geol. Soc. Am. Bull. 72, 193–286.

Evans, H.K., Hall, I.R., Bianchi, G.G., Oppo, D.W., 2007. Intermediate water links to Deep Western Boundary current variability in the subtropical NW Atlantic during Marine Isotope stages 5 and 4. Paleoceanography 22. http://dx.doi.org/10.1029/2006PA001409.

Exon, N.F., Hill, P.J., Mitchell, C., Post, A., 2005. Nature and origin of the submarine Albany canyons off southwest Australia. Aust. J. Earth Sci. 52, 101–115.

Grammer, G.M., Ginsburg, R.N., 1992. Highstand versus lowstand deposition on carbonate platform margins: insight from Quaternary foreslopes in the Bahamas. Mar. Geol. 103, 125–136.

Harris, P.T., Whiteway, T., 2011. Global distribution of large submarine canyons: geomorphic differences between active and passive continental margins. Mar. Geol. 285, 69–86.

Harwood, G.M., Towers, P.A., 1988. Seismic sedimentological interpretation of a carbonate slope, north margin of Little Bahama Bank. In: Proc. ODP Sci. Results. *vol.* 101. pp. 263–277.

Heath, K.C., Mullins, H.T., 1984. Open-ocean, off-bank transport of fine-grained carbonate sediment in the Northern Bahamas. Geol. Soc. Lond., Spec. Publ. 15, 199–208.

Huneke, H., Mulder, T., 2010. Deep-sea Sediments. Elsevier.

Jo, A., Eberli, G.P., Grasmueck, M., 2015. Margin collapse and slope failure along southwestern Great Bahama Bank. Sediment. Geol. 317, 43–52.

Jobe, Z.R., Lowe, D.R., Uchytil, S.J., 2011. Two fundamentally different types of submarine canyons along the continental margin of Equatorial Guinea. Mar. Pet. Geol. 28, 843–860.

Jorry, S.J., Droxler, A.W., Francis, J.M., 2010. Deepwater carbonate deposition in response to re-flooding of carbonate bank and atoll-tops at glacial terminations. Quat. Sci. Rev. 29, 2010–2026.

Kaczmarek, S.E., Hicks, M.K., Fullmer, S.M., Steffen, K.L., Bachtel, S.L., 2010. Mapping facies distributions on modern carbonate platforms through integration of multispectral Landsat data, statistics-based unsupervised classifications, and surface sediment data. AAPG Bull. 94, 1581–1606.

Lewis, K.B., Barnes, P.M., 1999. Kaikoura Canyon, New Zealand: active conduit from near-shore sediment zones to trench-axis channel. Mar. Geol. 162, 39–69.

Malone, M.J., Slowey, N.C., Henderson, G.M., 2001. Early diagenesis of shallow-water periplatform carbonate sediments, leeward margin, Great Bahama Bank (Ocean Drilling Program Leg 166). Geol. Soc. Am. Bull. 113, 881–894.

Mazières, A., Gillet, H., Castelle, B., Mulder, T., Guyot, C., Garlan, T., Mallet, C., 2014. High-resolution morphobathymetric analysis and evolution of Capbreton submarine canyon head (Southeast Bay of Biscay—French Atlantic Coast) over the last decade using descriptive and numerical modeling. Mar. Geol. 351, 1–12.

McNeill, D.F., Grammer, G.M., Williams, S.C., 1998. A 5 MY chronology of carbonate platform margin aggradation, southwestern Little Bahama Bank, Bahamas. J. Sediment. Res. 68, 603–614.

Mitchell, J.K., Holdgate, G.R., Wallace, M.W., Gallagher, S.J., 2007. Marine geology of the Quaternary Bass Canyon system, southeast Australia: a cool-water carbonate system. Mar. Geol. 237, 71–96.

Mulder, T., Syvitski, J.P.M., Migeon, S., Faugères, J.-C., Savoye, B., 2003. Marine hyperpycnal flows: initiation, behavior and related deposits. a review. Mar. Pet. Geol. 20, 861–882.

Mulder, T., Ducassou, E., Eberli, G.P., Hanquiez, V., Gonthier, E., Kindler, P., Principaud, M., Fournier, F., Léonide, P., Billeaud, I., Marsset, B., Reijmer, J.J.G., Bondu, C., Joussiaume, R., Pakiades, M., 2012a. New insights into the morphology and sedimentary processes along the western slope of Great Bahama Bank. Geology 40, 603–606.

Mulder, T., Ducassou, E., Gillet, H., Hanquiez, V., Tournadour, E., Combes, J., Eberli, G.P., Kindler, P., Gonthier, E., Conesa, G., Robin, C., Sianipar, R., Reijmer, J.J.G., François, A., 2012b. Canyon morphology on a modern carbonate slope of the Bahamas: evidence of a regional tectonic tilting. Geology 40, 771–774.

Mulder, T., Joumes, M., Hanquiez, V., Gillet, H., Reijmer, J.J.G., Tournadour, E., Chabaud, L., Principaud, M., Schnyder, J.S.D., Borgomano, J., Fauquembergue, K., Ducassou, E., Busson, J., 2017. Carbonate slope morphology revealing sediment transfer from bank-to-slope (Little Bahama Bank, Bahamas). Mar. Pet. Geol. 83, 26–34.

Mullins, H.T., Mark Van Buren, H., 1981. Walkers Cay Fault, Bahamas: Evidence for Cenozoic faulting. Geo-Marine Letters 1 (3), 225–231.

Mullins, H.T., Neumann, A.C., 1979. Deep carbonate bank margin structure and sedimentation in the Northern Bahamas. In: Geology of Continental Slopes. vol. 27. SEPM Society for Sedimentary Geology, pp. 165–192.

Mullins, H.T., Keller, G.H., Kofoed, J.W., Lambert, D.N., Stubblefield, W.L., Warme, J.E., 1982. Geology of Great Abaco Submarine Canyon (Blake Plateau): observations from the research submersible “Alvin”. Mar. Geol. 48, 239–257.

Mullins, H.T., Heath, K.C., Van Buren, H.M., Newton, C.R., 1984. Anatomy of a modern open-ocean carbonate slope: northern Little Bahama Bank. Sedimentology 31, 141–168.

Neumann, A.C., Land, L.S., 1975. Lime mud deposition and calcareous algae in the Bight of Abaco, Bahamas; a budget. J. Sediment. Res. 45, 763–786.

Normark, W.R., Carlson, P.R., 2003. Giant submarine canyons: is size any clue to their importance in the rock record? Geol. Soc. Am. Spec. Pap. 370, 175–190.

Pratson, L.F., Coakley, B.J., 1996. A model for the headward erosion of submarine canyons induced by downslope-eroding sediment flows. Geol. Soc. Am. Bull. 108, 225–234.

Pratson, L.F., Ryan, W.B.F., Mountain, G.S., Twichell, D.C., 1994. Submarine canyon initiation by downslope-eroding sediment flows: evidence in late Cenozoic strata on the New Jersey continental slope. Geol. Soc. Am. Bull. 106, 395–412.

Principaud, M., Mulder, T., Gillet, H., Borgomano, J., 2015. Large-scale carbonate submarine mass-wasting along the northwestern slope of the Great Bahama Bank (Bahamas): morphology, architecture, and mechanisms. Sediment. Geol. 317, 27–42.

Principaud, M., Ponte, J.-P., Mulder, T., Gillet, H., Robin, C., Borgomano, J., 2016. Slope-to-basin stratigraphic evolution of the northwestern Great Bahama Bank (Bahamas) during the Neogene to Quaternary: interactions between downslope and bottom

currents deposits. Basin Res (in press).
Puga-Bernabéu, Á., Webster, J.M., Beaman, R.J., Guilbaud, V., 2011. Morphology and controls on the evolution of a mixed carbonate–siliciclastic submarine canyon system, Great Barrier Reef margin, north-eastern Australia. Mar. Geol. 289, 100–116.
Puga-Bernabéu, Á., Webster, J.M., Beaman, R.J., Guilbaud, V., 2013. Variation in canyon morphology on the Great Barrier Reef margin, north-eastern Australia: the influence of slope and barrier reefs. Geomorphology 191, 35–50.
Puga-Bernabéu, Á., Webster, J.M., Beaman, R.J., Reimer, P.J., Renema, W., 2014. Filling the gap: a 60 ky record of mixed carbonate-siliciclastic turbidite deposition from the Great Barrier Reef. Mar. Pet. Geol. 50, 40–50.
Purkis, S.J., Harris, P.M., 2016. The extent and patterns of sediment filling of accommodation space on great Bahama Bank. J. Sediment. Res. 86, 294–310.
Rankey, E.C., Doolittle, D.F., 2012. Geomorphology of carbonate platform-marginal uppermost slopes: insights from a Holocene analogue, Little Bahama Bank, Bahamas. Sedimentology 7, 2146–2171.
Rankey, E.C., Doolittle, D.F., 2012. Geomorphology of carbonate platform-marginal uppermost slopes: insights from a Holocene analogue, Little Bahama Bank, Bahamas. Sedimentology.
Ravenne, C., Le Quellec, P., Valery, P., 1985. Dépôts carbonatés profonds des Bahamas. In: Géodynamique des caraïbes. Symposium. Edition Technip, Paris, pp. 255–271.
Reeder, S.L., Rankey, E.C., 2008. Interactions between tidal flows and ooid shoals, Northern Bahamas. J. Sediment. Res. 78, 175–186.
Reeder, S.L., Rankey, E.C., 2009. Controls on morphology and sedimentology of carbonate tidal deltas, Abacos, Bahamas. Mar. Geol. 267, 141–155.
Schlager, W., Ginsburg, R.N., 1981. Bahama carbonate platforms-the deep and the past. Mar. Geol. 44, 1–24.
Schlager, W., James, N.P., 1978. Low-magnesian calcite limestones forming at the deep-sea floor, Tongue of the Ocean, Bahamas. Sedimentology 25, 675–702.
Schlager, W., Bourgeois, F., Mackenzie, G., Smit, J., 1988. Boreholes at Great Isaac and Site 626 and the history of the Florida Straits. Proc., scientific results, ODP, Leg 101, Bahamas 425–437.
Schlager, W., Reijmer, J.J.G., Droxler, A., 1994. Highstand shedding of carbonate platforms. J. Sediment. Res. 64, 270–281.
Shepard, F.P., 1936. The underlying causes of submarine canyons. Proc. Natl. Acad. Sci. U. S. A. 22, 496–502.
Shepard, F.P., 1981. Submarine canyons; multiple causes and long-time persistence. AAPG Bull. 65, 1062–1077.
Shepard, F.P., Dill, R.F., Vonrad, U., 1969. Physiography and sedimentary processes of La Jolla submarine fan and fan-valley, California. AAPG Bull. 53, 390–420.
Tournadour, E., 2015. Architecture et dynamique sédimentaire d'une pente carbonatée moderne: exemple de la pente nord de Little Bahama Bank (LBB), Bahamas. Ed Bordeaux University.
Tournadour, E., Mulder, T., Borgomano, J., Hanquiez, V., Ducassou, E., Gillet, H., 2015. Origin and architecture of a Mass Transport Complex on the northwest slope of Little Bahama Bank (Bahamas): relations between off-bank transport, bottom current sedimentation and submarine landslides. Sediment. Geol. 317, 9–26.
Van Buren, H.M., Mullins, H.T., 1983. Seismic stratigraphy and geologic development of an open-ocean carbonate slope; the northern margin of Little Bahama Bank. In: Sheridan, R.E., Gradstein, F.M. (Eds.), Init. Repts. DSDP, 76. U.S. Govt. Printing Office, Washington, pp. 749–762.
Webster, J.M., Beaman, R.J., Puga-Bernabéu, Á., Ludman, D., Renema, W., Wust, R.A.J., George, N.P.J., Reimer, P.J., Jacobsen, G.E., Moss, P., 2012. Late Pleistocene history of turbidite sedimentation in a submarine canyon off the northern Great Barrier Reef, Australia. Palaeogeogr. Palaeoclimatol. Palaeoecol. 331–332, 75–89.
Wilson, P.A., Roberts, H.H., 1992. Carbonate-periplatform sedimentation by density flows: a mechanism for rapid off-bank and vertical transport of shallow-water fines. Geology 20, 713–716.
Wilson, P.A., Roberts, H.H., 1995. Density cascading; off-shelf sediment transport, evidence and implications, Bahama Banks. J. Sediment. Res. 65, 45–56.
Wunsch, M., Betzler, C., Lindhorst, S., Lüdmann, T., Eberli, G.P., 2017. Sedimentary dynamics along carbonate slopes (Bahamas archipelago). Sedimentology 64, 631–657.